Human spinal cord differentiation proceeds rapidly in vitro and only initially maintains differentiation pace in a heterologous environment

Alwyn Dady*, Lindsay Davidson, Pamela A. Halley and Kate G. Storey*

Division of Cell & Developmental Biology, School of Life Sciences,

University of Dundee, Dundee DD1 5EH, UK

* corresponding authors

Key words: human pluripotent cells, human spinal cord development, neural differentiation timing, xenografting,

Abstract

Species-specific differentiation pace in in vitro assays indicates that some aspects of neural differentiation are driven by cell-autonomous processes. Here we describe a novel in vitro human neural rosette assay that recapitulates the temporal sequence of dorsal spinal cord differentiation but proceeds more rapidly than in the human embryonic spinal cord, suggesting that in vitro conditions lack endogenous signalling dynamics. To test the extent to which this in vitro assay represents a cell intrinsic differentiation programme, human iPSC-derived neural rosettes were homo-chronically grafted into the faster differentiating chicken embryonic neural tube. Strikingly, in vitro human differentiation pace was not accelerated, even in single host-integrated cells. Moreover, rosette differentiation eventually stalled in a neural progenitor cell state. These findings demonstrate the requirement for timely extrinsic signalling to accurately recapitulate human neural differentiation tempo, and suggest that while intrinsic properties limit differentiation pace, such signals are also required to maintain differentiation progression.

150

Introduction

Understanding human embryonic development is a major challenge in contemporary biology and is in large part investigated by creation of pluripotent cell derived in vitro models of developing tissues and organs. One of the most striking features of such in vitro assays is the remarkably faithful recapitulation of specific differentiation programmes in minimal culture conditions. For example, species specific patterns of cell proliferation and timing of neuronal sub-type differentiation are evident in human and macaque cortical progenitors, even when these cells are cultured together (Otani et al. 2016), strongly supporting the notion that cell autonomous mechanisms direct differentiation programmes. Recent analyses of potential mechanisms that account for human specific differentiation tempo have identified general protein stability and cell cycle duration as parameters that constrain this process in spinal cord progenitors (Rayon et al. 2020). Moreover, a human specific gene, *ARHGAP11B*, has recently been shown to promote the enhanced proliferative capacity of human basal cortical progenitors by augmenting a specific metabolic pathway (Namba et al. 2020): and so uncovering a genetic basis for such cell autonomous cell behaviour. Such findings indicate that cell intrinsic mechanisms underpin differentiation programme progression and suggest that this process can proceed from the neural progenitor cell state with minimal extrinsic signals. Evaluation of the extent to which human neural progenitors differentiate cell autonomously requires a detailed understanding of the differentiation timing of specific cell types during normal human embryogenesis and how well this is recapitulated in vitro.

As in other vertebrate embryos, the extracellular environment, including spatially and temporally regulated signals provided by neighbouring tissues, is likely to orchestrate human embryonic differentiation. In vitro models, from rosettes to more complex three-dimensional organoids and gastruloids, aim to recreate this by provision of supportive extracellular environments and timely exposure to ligands or small molecules that modulate signalling activity (Lancaster et al. 2013, Otani et al. 2016, Ogura et al. 2018, Chiaradia and Lancaster 2020, Moris et al. 2020). A critical test of the extent to which neural progenitor differentiation is governed by cell autonomous mechanisms is their behaviour in a heterologous environment. However, studies examining differentiation pace and accuracy in such contexts are lacking. This is obviously important when considering use of such neural progenitors in cell replacement strategies following injury or disease (Sofroniew 2018) or for local delivery of secreted factors for therapeutic effect (Zhang et al. 2017), as these approaches involve transplantation into heterologous environments and yet anticipate differentiation into specific cell types, e.g. (Kumamaru et al. 2018, Kumamaru et al. 2019).

A relatively simple region of the developing nervous system in which to evaluate the extent to which human neural progenitors differentiate cell autonomously, is the developing spinal cord. In vitro generation of spinal cord progenitors from mammalian pluripotent cells has been achieved by approaches in which anterior neural tissue is induced and then caudalised, e.g. (Meinhardt et al. 2014, Gupta et al. 2018). Recent advances in understanding the cellular origins of the spinal cord have further shown that it arises from a bipotent epiblast cell population adjacent to the anterior primitive streak known as neuromesodermal progenitors (NMPs) (Tzouanacou et al. 2009, Gouti et al. 2014, Gouti, Metzis, and Briscoe 2015, Henrique et al. 2015, Gouti et al. 2017, Steventon and Martinez Arias 2017). Moreover, in vitro generation of spinal cord progenitors from NMPs may align better with the temporal sequence of cell fate decisions in the embryo. Derivation of NMP-like cells from pluripotent cells has been demonstrated (Turner et al. 2014, Gouti et al. 2017, Frith et al. 2018, Verrier et al. 2018, Frith and Tsakiridis 2019, Edri et al. 2019) and this has catalysed investigation of mechanisms regulating human as well as mouse spinal cord development.

Here we present a novel human pluripotent cell-derived in vitro neural rosette assay that recapitulates dorsal spinal cord differentiation observed in vertebrate embryos and use this to evaluate to the extent to which human neural progenitors differentiate cell autonomously. Using key cell type-specific marker proteins we compare in detail in vitro neural differentiation with that in the human embryonic spinal cord. In a series of grafting experiments, in which human iPSC derived spinal cord progenitors are transplanted into the chicken embryonic neural tube, we further test whether human differentiation pace can be increased in this faster differentiating environment, as well as the extent to which the differentiation trajectory of transplanted cells relies on timely provision of extrinsic signalling.

Results

In vitro generation of human dorsal spinal cord rosettes

An in vitro protocol which generates dorsal spinal cord from human pluripotent cell-derived NMP-like cells with brachial/ thoracic character (Verrier et al. 2018) was used to make neural rosettes (Fig. 1A). The precise timing with which NMP-like cells (derived from H9 hESCs) enter the neural differentiation programme was assessed by quantifying cells expressing a range of neural progenitor markers during the first 10 days of two-dimensional culture in a minimal medium (Figs. 1A,B). This early neural tissue formed compact condensations of cells by day 4 (D4) of NMP-like cell differentiation, which lacked overt apico-basal polarity as indicated by localisation of N-Cadherin (Cadherin-2) at most cell-cell interfaces (Hatta and Takeichi 1986, Dady, Blavet, and Duband 2012) (Fig. 1B). These cells expressed SOX2, characteristic of both pluripotent, NMP and neural progenitor cells (Uchikawa et al. 2003, Uchikawa et al. 2011, Bylund et al. 2003) (Ellis et al. 2004), and the neural progenitor protein PAX6 (Walther and Gruss 1991, Pevny et al. 1998). Some cells expressing the early neural crest marker SNAI2 were also detected on D4 (Nieto 2002, Jiang et al. 2009, Dady and Duband 2017) (Fig. 1B). The expression of PAX7, which distinguishes dorsal neural progenitors (Jostes, Walther, and Gruss 1990) (Gruss and Walther 1992) and the absence of OLIG2, characteristic of more ventral spinal cord (Mizuguchi et al. 2001, Novitch, Chen, and Jessell 2001) further indicated that at D4 this differentiation protocol had generated human neural tissue with dorsal spinal cord identity (Fig. 1B).

By D6 neural rosettes composed of apico-basally polarised SOX2, PAX6 and PAX7 expressing progenitors had formed, with a single, central lumen and peripheral SNAI2 neural crest cells (Fig. 1B). This spatial reorganisation was accompanied by decline in SNAI2+ cells and the appearance, by D10, of a scattering of OLIG2 expressing cells (Fig. 1B). This emergence of neural rosettes from a condensing epiblast cell population at D4, may equate to the formation of the neural plate and establishment of the pseudostratified neuroepithelium, but it is also reminiscent of the phases of embryonic secondary neurulation (Schoenwolf and Nichols 1984, Catala, Teillet, and Le Douarin 1995, Dady, Blavet, and Duband 2012, Dady et al. 2014, Fedorova et al. 2019).

These findings show that differentiation of human ESC derived NMPs in a minimal culture medium containing retinoic acid (RA) is sufficient to generate self-organising dorsal spinal cord rosettes and accompanying neural crest. Moreover, this protocol induced similar dorsal spinal cord differentiation in hiPSC-derived NMP-like cells (Fig. S2).

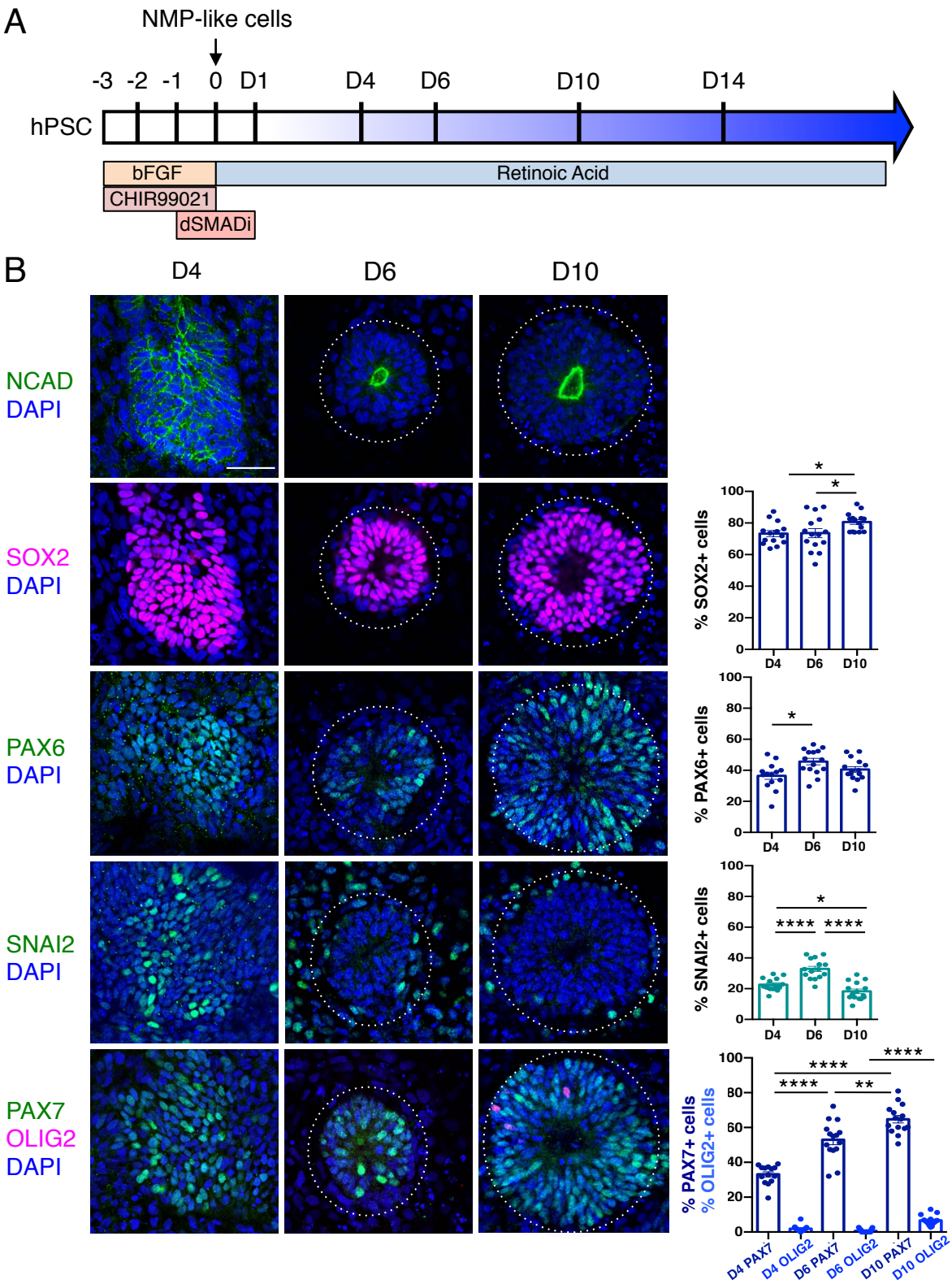

Figure 1. Human pluripotent cell derivation of NMP-like cells and their differentiation into dorsal spinal cord neural rosettes. (**A**) Timeline and protocol for induction and differentiation of dorsal spinal cord neural rosette from human pluripotent stem cells (hPSC); (**B**) Expression patterns and quantification of cell type specific proteins in rosettes on days (D)4, D6 and D10 detected by immunofluorescence combined with heterochromatin marker DAPI: apical polarity marker N-Cadherin (NCAD), neural progenitor markers SOX2, PAX6, early neural crest marker SNAI2, and dorso-ventrally restricted neural progenitor markers PAX7 and OLIG2. Quantifications indicate proportions of expressing cells in either a defined field on D4 or within a rosette D6 and D10, in 15 samples for each marker (n=5 from each of 3 independent differentiations, see Methods). Data analyzed with Mann-Whitney test, errors bars ± S.E.M, p-values = * $p < 0.05$, ** $p < 0.01$ and **** $p < 0.0001$. Scale bar = 50µm.

166 Sequential differentiation of human dorsal spinal cord progenitors is
167 recapitulated in vitro
168 Dorsal spinal cord rosettes were further characterized as they progressed through their
169 differentiation programmes (Fig. 2A). Decline of SNAI2-expressing cells at D10 coincided with
170 the emergence of migrating neural crest cells expressing HNK1 (Tucker et al. 1984, Bronner-
171 Fraser 1986), SOX10 (Bondurand et al. 1998) and TFAP2α (Zhang et al. 1996, Betters et al.
172 2010) in cells now just outside the rosettes (Jiang et al. 2009) (Fig. 2B). The onset of neuron
173 production was assessed in several ways; (i) by analysis of immature neuronal marker
174 Doublecortin (DCX) expression (Gleeson et al. 1999, Brown et al. 2003) (using a hESC (H1)
175 neuronal reporter cell line in which a yellow fluorescent protein (*YFP*) sequence is fused to
176 endogenous *DCX* (Yao et al. 2017) (Fig. 2C), and ii) by characterization of cdk inhibitor
177 P27/KIP1 expression, which identifies post-mitotic cells in the neural tube (Gui, Li, and Matise
178 2007) (Fig. 2D). These analyses defined a neurogenesis timeline which commenced by D8,
179 peaked at D14 and progressed through to D20.
180 By D20 DCX-expressing neurons largely resided at the rosette perimeter and the early
181 glial progenitor marker, the transcription factor Nuclear factor 1 A-type (NFIA) (Deneen et al.
182 2006), was now detected in cells within the rosette (Fig. 2C). This indicates operation of a
183 switch from neurogenic to gliogenic differentiation programmes in the human spinal cord
184 rosettes that is similar to that observed in the mouse embryo (Deneen et al. 2006).
185 Finally, we determined the identity of neurons generated in this in vitro assay by
186 immunofluorescence of dorsal interneuron (dIs) subtype-specific markers. In the mouse
187 embryonic neural tube distinct sensory interneurons arise in specific dorsoventral positions
188 and express distinguishing marker proteins (Lai, Seal, and Johnson 2016). By D10,
189 proprioceptive interneurons (dI1s) and mechanosensory interneurons (dI3s) were detected
190 by the expression of LHX2 (Fig. 2E) and ISLET1 (Fig. 2F), respectively (Liem, Tremml, and
191 Jessell 1997). By D14, dI5 interneurons expressing BRN3A were detected (Ninkina et al. 1993,
192 Fedtsova and Turner 1995) (Fig. 2G). Moreover, ISLET1+ cells did not co-express the
193 transcription factor HB9, a marker of spinal cord motoneurons (Arber et al. 1999), confirming
194 their dI3 identity (Fig. 2F). In contrast, LHX1/dI2s/dI4s expressing cells were not identified (Fig.
195 S1), indicating that this protocol is insufficient to generate all types of dorsal interneurons.
196 These data document the differentiation capacity in this human spinal cord rosette
197 assay and demonstrate that it reproducibly generates dorsal neural differentiation
198 programmes. These begin with dorsal neural progenitors and emerging neural crest, progress
199 to neurogenesis (of specific dorsal interneurons dI1s, dI3s and dI5s) and a later switch to

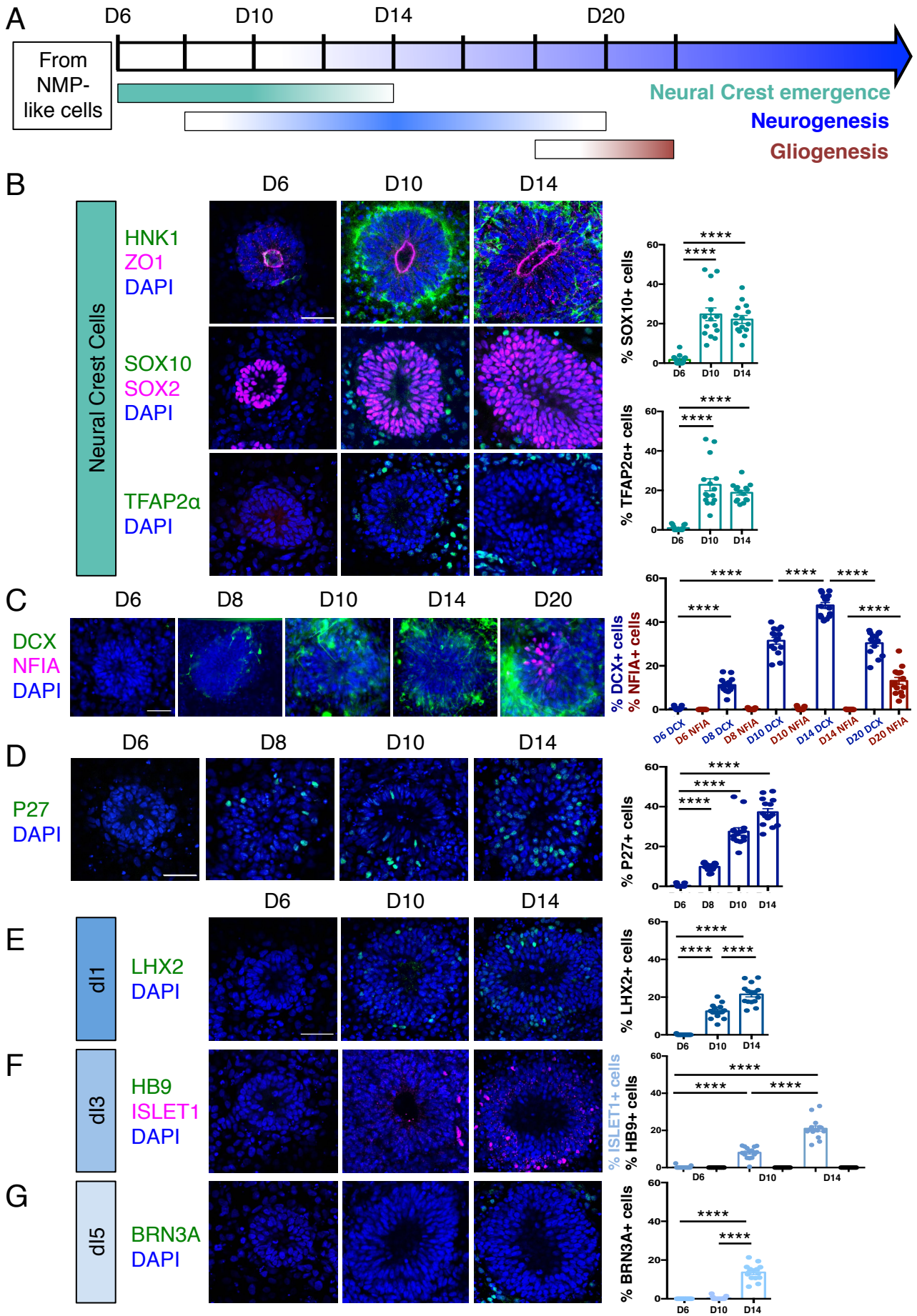

Figure 2. Human dorsal spinal cord rosettes exhibit stereotyped sequence of cell-type specific differentiation
(**A**) Schematic of in vitro sequence of cell-type specific differentiation of dorsal spinal cord rosettes; (**B**) Emergence of migrating neural crest from rosettes by D10, documented by IF for key marker proteins HNK1, (lumen defined by apical marker ZO-1), SOX10 (neural progenitors defined by SOX2) and TFAP2α and quantified for SOX10 and TFAP2α; (**C**) Transition from neurogenesis to gliogenesis documented and quantified in immature neuronal reporter line (H1:DCX-YFP) with co-IF for gliogenesis marker Nuclear Factor I-A (NFIA) at key timepoints; (**D**) P27/KIP1 expression which by analogy identifies most dorsal post-mitotic neurons, confirms neurogenesis onset by D8; (**E-G**) Emergence of dorsal interneuron (dIs) subtypes by D10 indicated by dI1s/LHX2 (**E**), dI3s/ISLET1 (**F**) (note lack of HB9/ ISLET1 co-expression distinguishes these cells from motor neurons) and dI5s/BRN3A (**G**). Sample numbers, statistics and error bars as in Figure 1, each dot represents a single rosette and see Materials and Methods; Scale bar = 50µm.

233 gliogenesis: a sequence that recapitulates the temporal order of differentiation observed in
234 the spinal cord of mouse and avian embryos (Fig. 2A) (Deneen et al. 2006, Glasgow et al.
235 2017, Andrews et al. 2017).
236

237 Human spinal cord differentiation in vitro progresses more rapidly than in the
238 human embryonic spinal cord

239 This conservation in the sequence of the dorsal neural differentiation programme contrasts
240 with the longer duration of human embryogenesis in comparison with that observed in the
241 mouse and chicken. Indeed, the pace of differentiation in the developing nervous system and
242 that of body axis segmentation is slower in human embryos (Rayon et al. 2020, Matsuda et al.
243 2020). These latter studies suggest the presence of species-specific cell intrinsic differences
244 that govern developmental tempo. To understand how well this tempo is captured in our in
245 vitro assay we next sought to compare the sequence and timing of differentiation progression
246 in human spinal cord rosettes with that observed in the human embryo.

247 The pattern and timing of key marker protein expression in human embryonic spinal
248 cord was assessed using a combination of tissue samples provided by the HDBR (Figs. 3A-H)
249 and available data. One way in which to assess differentiation progression is to take
250 advantage of the spatial separation of the temporal events of differentiation along the
251 embryonic body axis, and so analyses were carried out at distinct rostro-caudal levels in
252 Carnegie stage (CS) 12/13 (gestational weeks 4-4.5) human embryos (O'Rahilly 1987); sacral
253 (the most caudal and least differentiated region), lumbar and thoracic/brachial (more rostral
254 and most differentiated region). Developmental time along the body axis can be
255 approximated by that indicated by segmentation progression from the sacral to thoracic
256 region, which involves generation of ~20 somites (with 1 human somite generated every 5
257 hours (Turnpenny et al. 2007, Hubaud and Pourquié 2014, Matsuda et al. 2020) this
258 represents, 100h or ~4 days (Fig. 3A).

259 The sacral spinal cord at CS12/13 stage was composed of progenitors expressing
260 dorsal (PAX7) and ventral (OLIG2) markers (Fig. 3B) as well as pre-migratory neural crest cells
261 expressing SNAI2 (Fig. 3C) and lacking migratory neural crest cell marker HNK1 (Fig. 3D).
262 Moreover, neurogenesis, revealed by the pan-neuronal marker TUJ1, was only detected
263 ventrally (Menezes and Luskin 1994) (Figs. 3E). The differentiation state in the dorsal region
264 of the CS12/13 sacral neural tube therefore aligns well with that found in D6 dorsal spinal
265 cord rosettes, which constitute apico-basally polarised neuroepithelium expressing PAX6,
266 PAX7 and SNAI2 (Fig. 1B) that lacks migratory neural crest and neurons (Figs 2B-G).

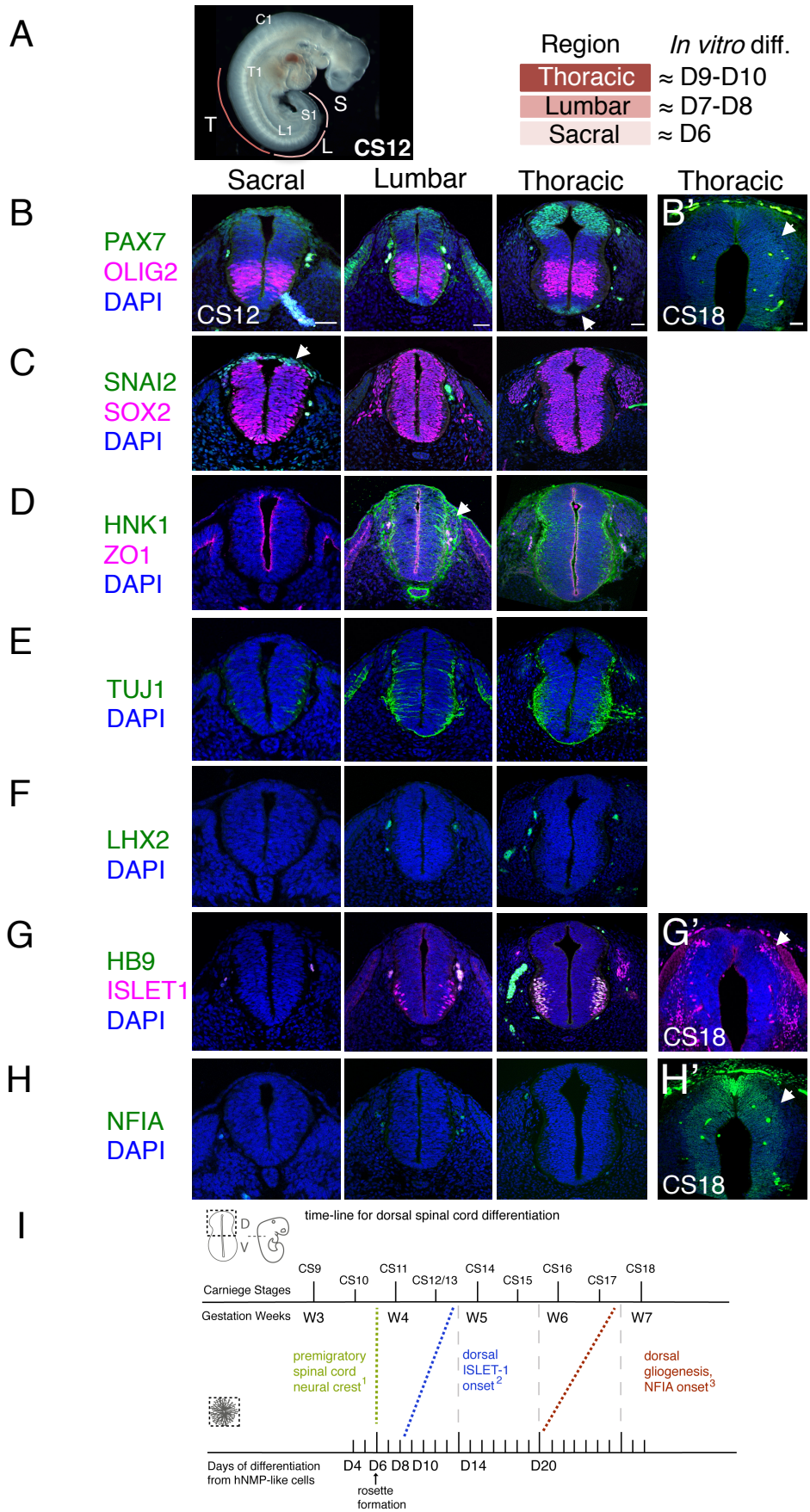

Figure 3 Characterization of neural progenitors and neuronal subtypes in human embryonic spinal cord and comparison with in vitro neural rosette differentiation. (**A**) CS12 human embryo with anatomical sub-regions indicated and their alignment with in vitro spinal cord rosette differentiation (see text); (**B-H**) transverse sections through human embryonic spinal cord at sacral, lumbar and thoracic levels at 4/4.5 weeks (CS12/CS13) and at brachial/thoracic at 7/7.5 weeks (CS18) analysed by IF for expression of (**B and B'**) dorsal, PAX7, or ventral, OLIG2, spinal cord progenitor markers (note novel PAX7 detection in the floor plate, arrow) and (**B'**) waning PAX7 at CS18 (arrow); (**C**) premigratory neural crest cell marker SNAI2 is only detected in sacral regions (arrow) shown here with pan-neural progenitor marker SOX2; (**D**) differentiating migrating neural crest expressing HNK1 emerges from the lumbar region (arrow); (**E**) neuronal differentiation detected with pan-neuronal marker TUJ1 is manifest dorsally in lumbar regions; dorsal interneurons indicated by (**F**) dI1 specific transcription factor LHX2 and (**G**) dI3 identifying ISLET1 expressing cells were not detected dorsally in any region of the spinal cord at CS12/CS13; (G') dorsal ISLET1 interneurons at CS18; (**H, H'**) gliogenesis marker NFIA detected dorsally only at CS18; (**I**) Schematic aligning dorsal brachial/thoracic spinal cord differentiation in human embryo and in hPSC derived dorsal spinal cord rosettes, based on (1) Bondurand N. et al. 1998, O'Rahilly and Müller 2007; (2) This study, Rayon T. et al. 2020, Marklund et al 2014; (3) This study, Rayon T. et al. 2020); three sections were analysed at each level for each marker in n = 2 CS12/13 and n = 1 CS18 human embryos. Scale bar = 50µm.

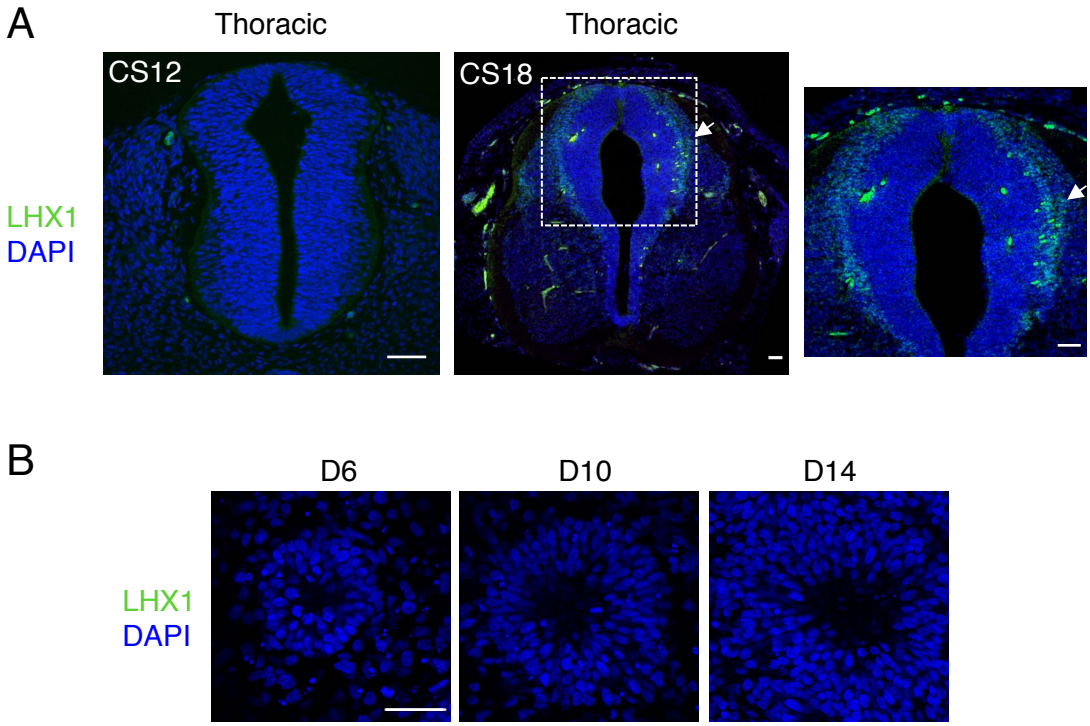

Figure S1. **Dorsal interneurons type 2 expressing LHX1, dI2/LHX1, are not generated in human spinal cord neural rosettes in vitro**. (**A**) dI2 neuron differentiation analysed by IF for expression of LHX1 in stages CS12 and CS18 human embryonic spinal cord; note dI2 neurons are only detected at CS18 (arrow indicates LHX1 expressing cells, dashed white boxes indicate area of magnification in next adjacent image); (**B**) LHX1 is not detected in neural rosettes differentiated in vitro. Three sections were analysed at each stage in n = 1 CS12 n=1 CS13 and n =1 CS18 human embryos. Three independent cell differentiations were performed to generate rosettes. Five neural rosettes from each experiment were then analysed for quantification at each time point (n=15). Data were analysed using non-parametric Mann-Whitney test. Scale bar = 50µm

334 In the more rostral, lumbar region, PAX7 and OLIG2 domains have enlarged
335 (Marklund et al. 2014) and, while SNAI2-expression has declined (Fig. 3C), migrating HNK1-
336 expressing neural crest cells have now emerged (Fig. 3D). The first neurons are now detected
337 in the dorsal half of the neural tube as indicated by TUJ1 expression (while co-expression of
338 ISLET1 and HB9 identifies ventrally located motor-neurons (Arber et al. 1999, Rayon et al.
339 2020), Figs. 3E, G). The dorsal neurons may correspond to the DCX /P27 expressing cells
340 detected in D8 rosettes (Figs. 2C,D), however, their identity remains undefined. Neurons in
341 this dorsoventral position (ventral region of dorsal half of the neural tube) in the mouse and
342 chicken neural tube express LHX1 (Lai, Seal, and Johnson 2016, Andrews et al. 2017), but this
343 protein was not detected in neural rosettes and appears much later in the human embryo
344 (Fig. S1). Given the alteration in transcription factor combinatorial code created by the
345 expansion of the OLIG2 domain in human spinal cord progenitors (Marklund et al. 2014), one
346 possibility is that human-specific neuronal cell types arise in this region. The dorsal region of
347 the lumbar neural tube therefore broadly aligns with D8-D10 dorsal spinal cord rosettes in
348 which neuronal differentiation and neural crest migration have now commenced (Figs. 2B-D).
349 Importantly, dorsal interneurons dI1 and dI3 indicated by LHX2 and ISLET1/HB9-
350 expression respectively were not detected in the human CS12 or CS13 embryonic spinal cord
351 at lumbar or the thoracic levels assessed here (which included sections from presumptive
352 forelimb level, brachial spinal cord), (Figs. 3F, G), although a few dorsal ISLET1 positive cells
353 were detected in brachial spinal cord of a further CS13 embryo (T. Rayon pers comm.). This
354 suggests that these interneurons are just beginning to be generated at CS13. In contrast,
355 ISLET1 and LHX2 positive cells were found in all D10 neural rosettes (Figs. 2E, F). This suggests
356 that the dorsal interneuron differentiation programme progresses more rapidly in vitro than
357 in the human embryonic spinal cord.
358 A further way to assess differentiation tempo is to align progression of a defined cell
359 population in vitro and in vivo using time elapsed from a key landmark event. The NMP-like
360 cells generated in our protocol have a brachial/thoracic regional character as indicated by Hox
361 gene expression (Verrier et al. 2018) and differentiation of this region can be compared in
362 vitro and in embryos over time. Detailed analysis of the first appearance of spinal cord neural
363 crest in the human embryo provides a clear landmark with which to align in vivo and in vitro
364 differentiation (Bondurand et al. 1998, O'Rahilly and Muller 2007). These latter studies
365 identify morphological emergence of migrating neural crest in cervical level spinal cord at
366 CS11 human embryo (O'Rahilly and Muller 2007) and in even more caudal spinal cord at this
367 stage using *SOX10 mRNA* expression (Bondurand et al. 1998). From this we infer that pre-

368 migratory neural crest is present prior to CS11 in brachial/thoracic spinal cord, and so aligns
369 this region in CS10-11 embryos with D6 in our neural rosettes, which express SNAI2 but lack
370 migratory neural crest markers proteins SOX10, HNK1 and TFAP2α (Figure 1B and 2B). Using
371 this alignment point we then compared time to appearance of later cell type specific markers
372 in neural rosettes and human embryos (Fig.3I). As above, dorsally located ISLET1/dI3s first
373 appear ~ CS13 and are robustly detected at CS15 ((Rayon et al. 2020); and see HDBR Atlas
374 http://hdbratlas.org), and here this indicates that these neurons appear at least ~4 days
375 earlier in D10 rosettes (Figs. 2E,F, 3I). The landmark switch from neurogenesis to gliogenesis
376 indicated by NFIA expression in dorsal neural progenitors was detected in human embryos at
377 CS18 (gestational weeks 7-7.5) (Fig. 3H') and not at CS17 (Rayon et al. 2020). This is ~ 1 week
378 later than in neural rosettes, where NFIA was robustly found at D20 (Figs. 2C, 3I). Moreover,
379 the overall time from spinal cord migratory neural crest appearance to dorsal gliogenesis
380 takes ~ 2 weeks (D6 -D20) in human dorsal spinal cord rosettes *in vitro* and ~ 3-3.5 weeks
381 (CS10/11-CS17/18) in the human embryonic spinal cord (Fig. 3I). These findings indicate that
382 in vitro conditions can alter the pace of neural differentiation progression, which proceeds
383 faster than in vivo within the context of these self-organizing neural rosettes.
384

385 Cell intrinsic differentiation of human spinal cord progenitors is unaltered by
386 differentiation cues from the more rapidly developing chicken embryonic
387 environment

388 In the vertebrate embryo, the timing of neural differentiation is orchestrated by signals from
389 adjacent tissues, which drive and coordinate axial differentiation (Diez del Corral, Breitkreuz,
390 and Storey 2002, Diez del Corral et al. 2003) but the localised and temporally controlled
391 characteristics of this regulatory influence are lacking in vitro. Indeed, in the embryo, neural
392 progenitors will generate more cells to make a bigger structure and so proliferative phases
393 that expand cell populations might be longer. We have found that the smaller rosette
394 structures generated in vitro differentiate more rapidly and this raises the possibility that
395 differentiation pace in this minimal assay reflects the species-specific intrinsic constraints on
396 this process (Rayon et al. 2020). To test whether rosette cells retain such a cell intrinsic
397 differentiation programme or if this can run still faster in a more rapidly developing embryo
398 that also provides a more coherent extracellular environment, we next homo-chronically
399 grafted human neural rosettes into the dorsal neural tube of the chicken embryo.
400 To this end, human iPSCs (Cellartis hIPS4 cell line engineered to express a plasma
401 membrane tagged GFP, ChiPS4-pmGFP, see Methods) were differentiated into NMPs and

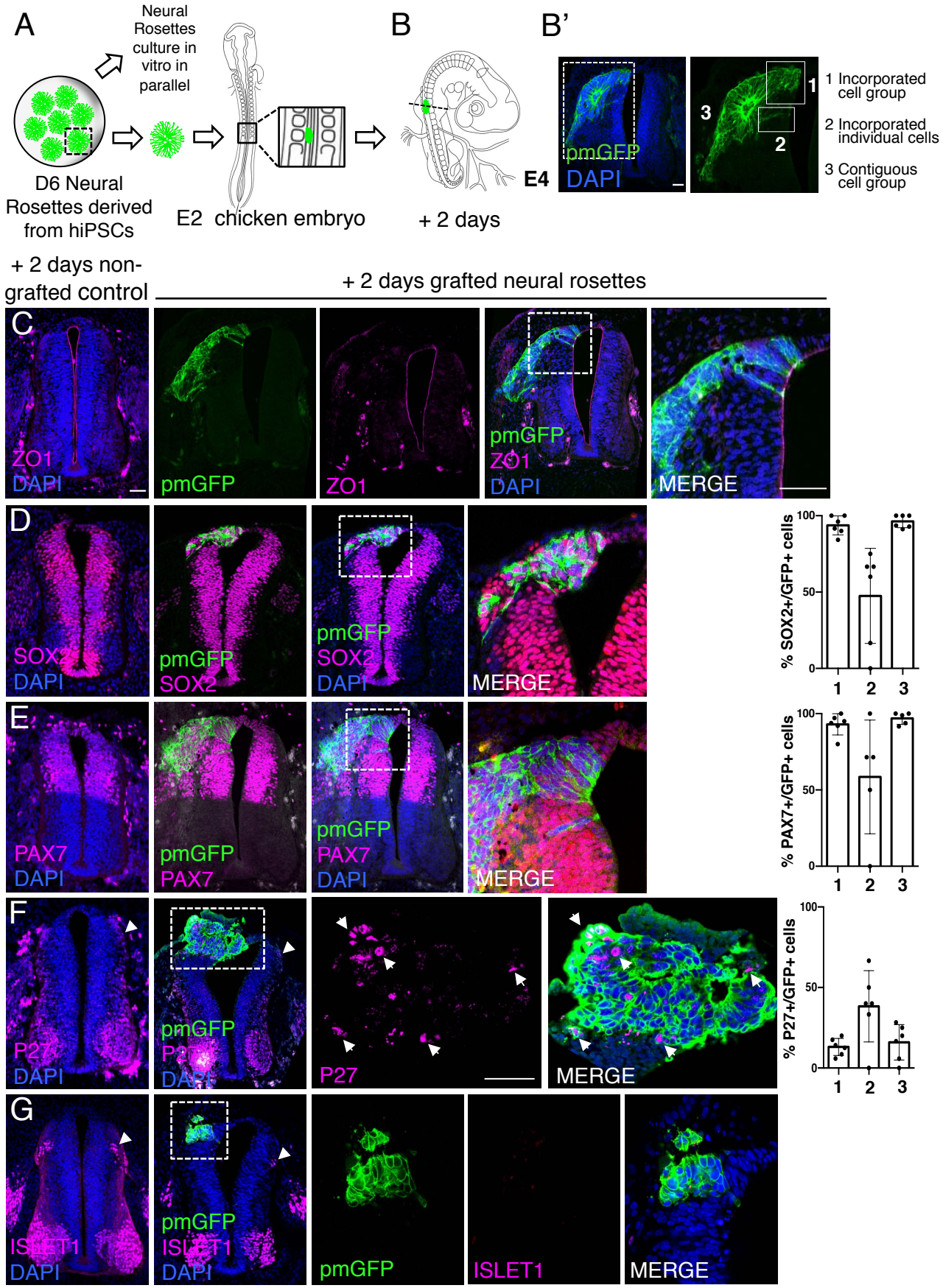

Figure 4. Homo-chronically transplanted hiPSC-derived neural rosettes exhibit cell autonomous differentiation despite exposure to more rapidly developing chicken embryonic environment. (**A**) Schematic of human dorsal spinal cord neural rosette transplantation experiment; (**B-B'**) Two days after grafting human cells were observed in: 1) cell groups or 2) isolated individual cells incorporated within the chicken neural tube, or 3) rosette-like configurations contiguous with chick neural tube. (**C-G**) IF to detect key marker proteins in control (non-grafted, note these sham operated embryos regenerate the dorsal neural tube by 2 days post-operation) and grafted embryos after 2 days incubation (**C**) ZO1, (**D**) SOX2, (**E**) PAX7, (**F**) P27, (**G**) ISLET1 (arrowheads indicate examples of candidate protein expressing cells in the chicken host tissue; arrow indicate example of P27 and GFP co-expressing cells, dashed white boxes indicate area of magnification in next adjacent image), three transverse sections from each of at least three grafted chicken embryos were analysed for each marker combination and the proportions of SOX2/GFP +ve, PAX7/GFP +ve and P27/GFP +ve cells in configurations 1, 2 or 3 were quantified, each dot represents data from one histological section, note the small number of isolated cells (group 2) underlies lack of significant difference between groups (see Materials and Methods), data analysed with Mann-Whitney U test with. Errors bars are ± SD. Scale bar = 50µm.

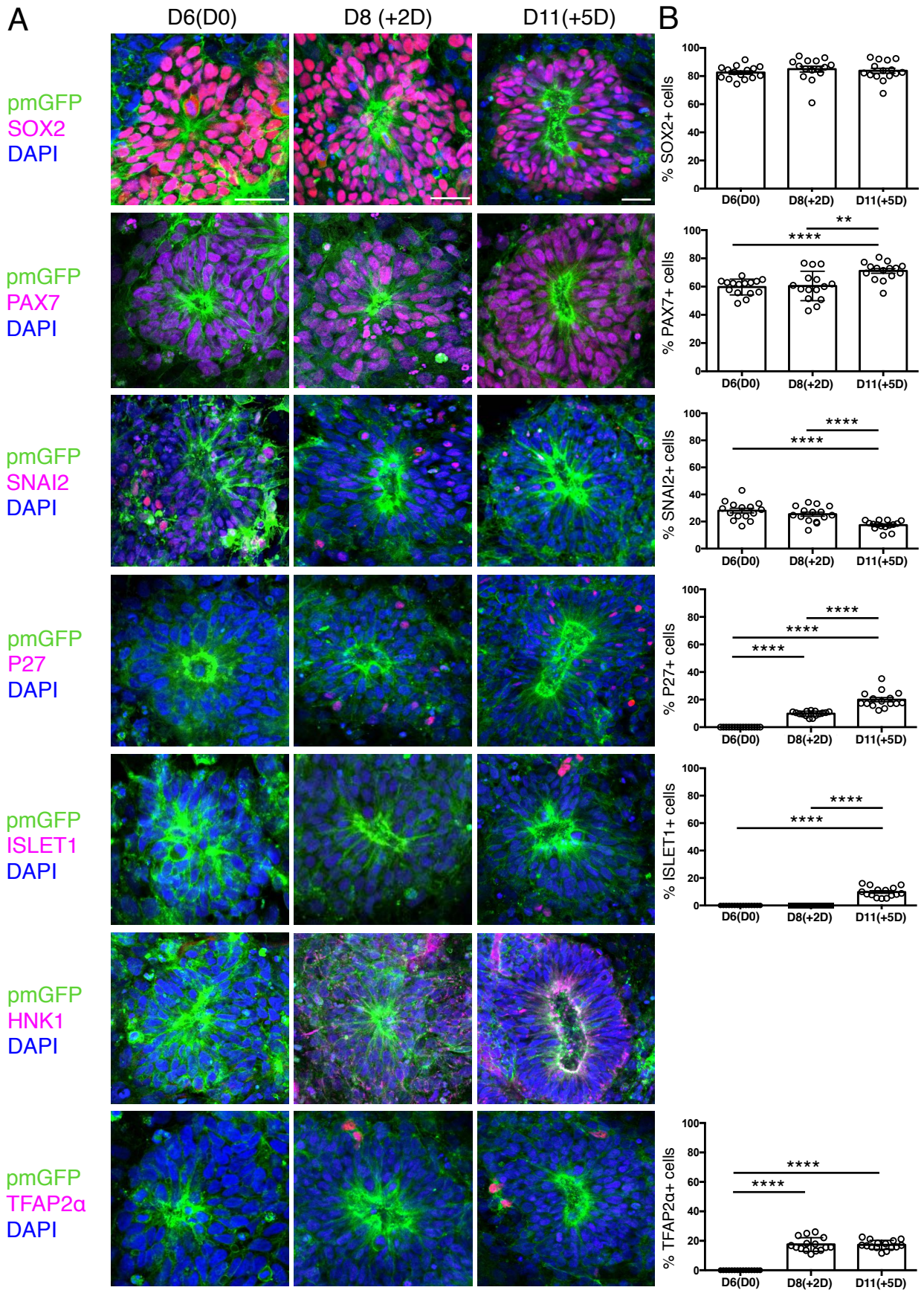

Figure S2. Expression patterns of key marker proteins in human dorsal spinal cord rosettes cultured in vitro in parallel with those homochronically grafted into chick spinal cord. (**A**) Human dorsal spinal cord rosettes from the same differentiation assays used for homochronic grafting experiments were cultured in parallel in vitro and subjected to IF for SOX2, PAX7, SNAI2, P27, ISLET1, HNK1 and TFAP2α SOX2, PAX7 and SNAI2 were expressed from D6(D0). P27, HNK1 and TFAP2α were detected from D8(+2D). ISLET1 was detected from D11(+5D). (**B**) Quantifications, percentage of cells in D6 rosettes expressing each marker on the day of grafting operation D6(D0), two Days after transplantation (+2D) which equals D8 in vitro, and five Days after transplantation (+5D), which equals D11 in vitro differentiation. Five rosettes from each of 3 independent differentiation experiments were used for quantifications, each dot represents data from a single rosette. See methods for statistical analysis. Errors bars are ± S.E.M. Probability of similarity, p-value ** $p < 0.01$ and **** $p < 0.0001$. Scale bar = 50µm.

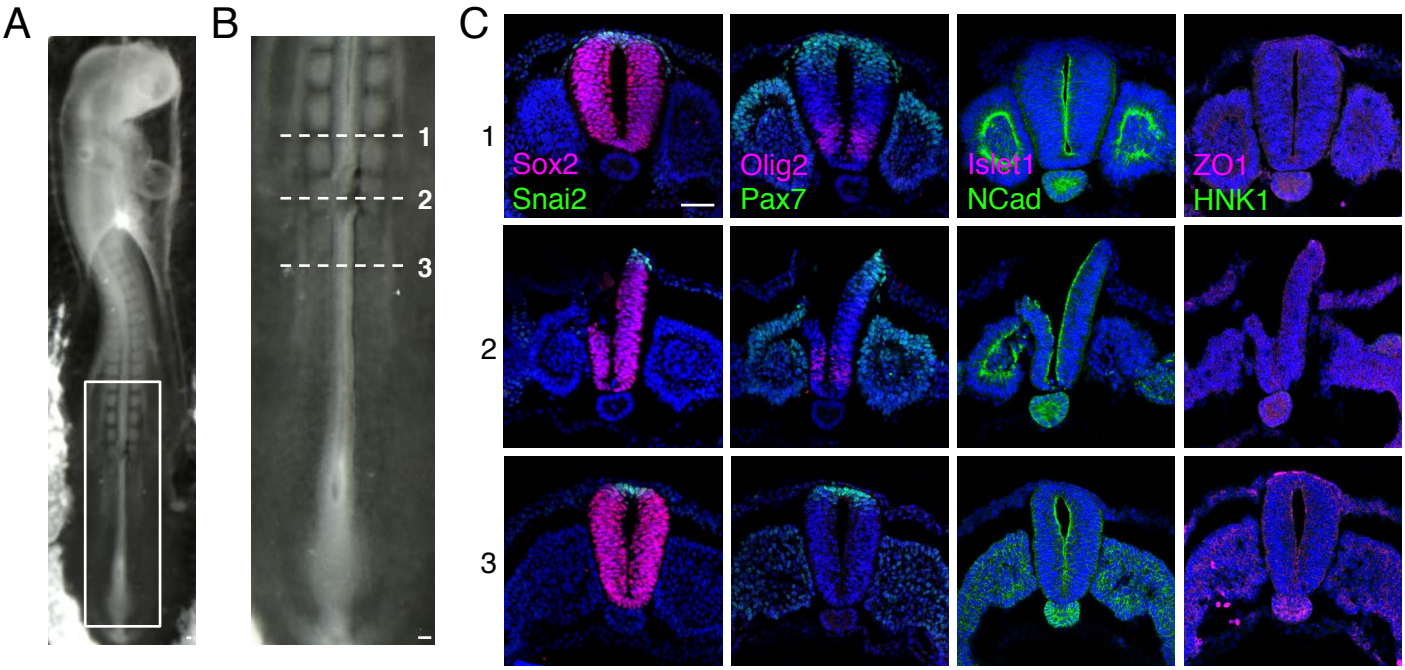

Figure S3. Dorsal region of the chicken neural tube removal prior to grafting. (**A**) E2 (10-15 somite stage, HH 10/11+) chicken embryo following removal of the dorsal part of neural tube. (**B**) High magnification of the newly formed somite region, where the dorsal part of the neural tube was surgically removed prior to grafting. (**C**) Transverse sections of chicken neural tube subjected to IF for SOX2, SNAI2, PAX7, OLIG2, ISLET1, NCAD, ZO1 and HNK1 in the region anterior to the removal site (1), the removal region (2), and the region caudal to the site (3). The neural tube region removed is only composed of neural crest and neural progenitors expressing respectively SNAI2 and PAX7 and is similar to D6 human spinal cord neural rosettes. At least three chicken embryos and three sections were analysed for each marker combination. Scale bar = 50µm.

503 then into D6 neural rosettes as described above (Fig. 1A). Multiple plates of rosettes were
504 generated so that control in vitro differentiation of iPSC derived rosettes was monitored in
505 parallel with that of D6 rosettes grafted into the chicken embryo. Expression of key marker
506 proteins in these iPSC derived rosettes was found to be the same as that in D6 rosettes
507 derived from the hESC H9 line (Fig. S2). Individual neural rosettes were micro-dissected,
508 lightly dissociated and grafted in place of one side of the dorsal neural tube adjacent to newly
509 formed somites in stage HH10-11 (Embryonic day 2, E2) chicken embryos (Figs. 4A, S3). At
510 this anatomical level the host chicken dorsal neural tube and grafted human D6 rosette are
511 composed of similar populations of dorsal neural progenitors and neural crest expressing
512 respectively PAX7 and SNAI2 and lack neurons and migrating neural crest (Figs. S2, S3);
513 moreover, the D6 rosettes which have brachial/thoracic regional character where grafted into
514 the corresponding region in the developing chicken embryo (opposite somites 10 - 16)
515 providing a regionally appropriate homochronic context in which evaluate differentiation
516 progression. After two days incubation, grafted cells retained apico-basal polarity as
517 indicated by localized ZO-1 and N-cadherin expression (Aaku-Saraste, Hellwig, and Huttner
518 1996, Hatta and Takeichi 1986, Dady, Blavet, and Duband 2012) (Fig. 4C) and the majority of
519 cells had formed rosette-like structures, which were adjacent but contiguous with the host
520 neuroepithelium, while subsets of cells were incorporated within the host neuroepithelium,
521 including some single cells (Figs. 4B, B'). At this time, most grafted cells still expressed neural
522 progenitor proteins (SOX2 and PAX7)(Figs. 4D, 4E) and the first P27 expressing neurons
523 appeared (Figs 4F and S2), but ISLET-1 expressing (dI3) interneurons were not yet detected
524 (Fig. 4G). This is in good alignment with neural differentiation progression observed in the
525 now D8 rosettes cultured in parallel in vitro (Fig. S2). Importantly, at this stage in the chicken
526 embryo ISLET-1/dI3 expressing neurons are detected (Fig. 4G) (Andrews et al. 2017),
527 consistent with the faster differentiation of the host tissue and indicating that the pace of
528 neural differentiation in grafted human rosettes is unaltered in this more rapidly
529 differentiating environment.
530 One possibility is that a community effect (Gurdon 1988) operates within grafted rosettes,
531 which overcomes differentiation signals provided by host tissues. We therefore analysed
532 separately human cells which were directly incorporated into the chick neuroepithelium,
533 either in small groups or as single cells to determine if these differentiated more rapidly (Fig.
534 4B'). However, no differences were found between contiguous rosettes and incorporated
535 human cell groups (Figs. 4D-G), and in single cells a slight tendency for reduced progenitor
536 marker expression and increased incidence of P27 was not statistically significant.

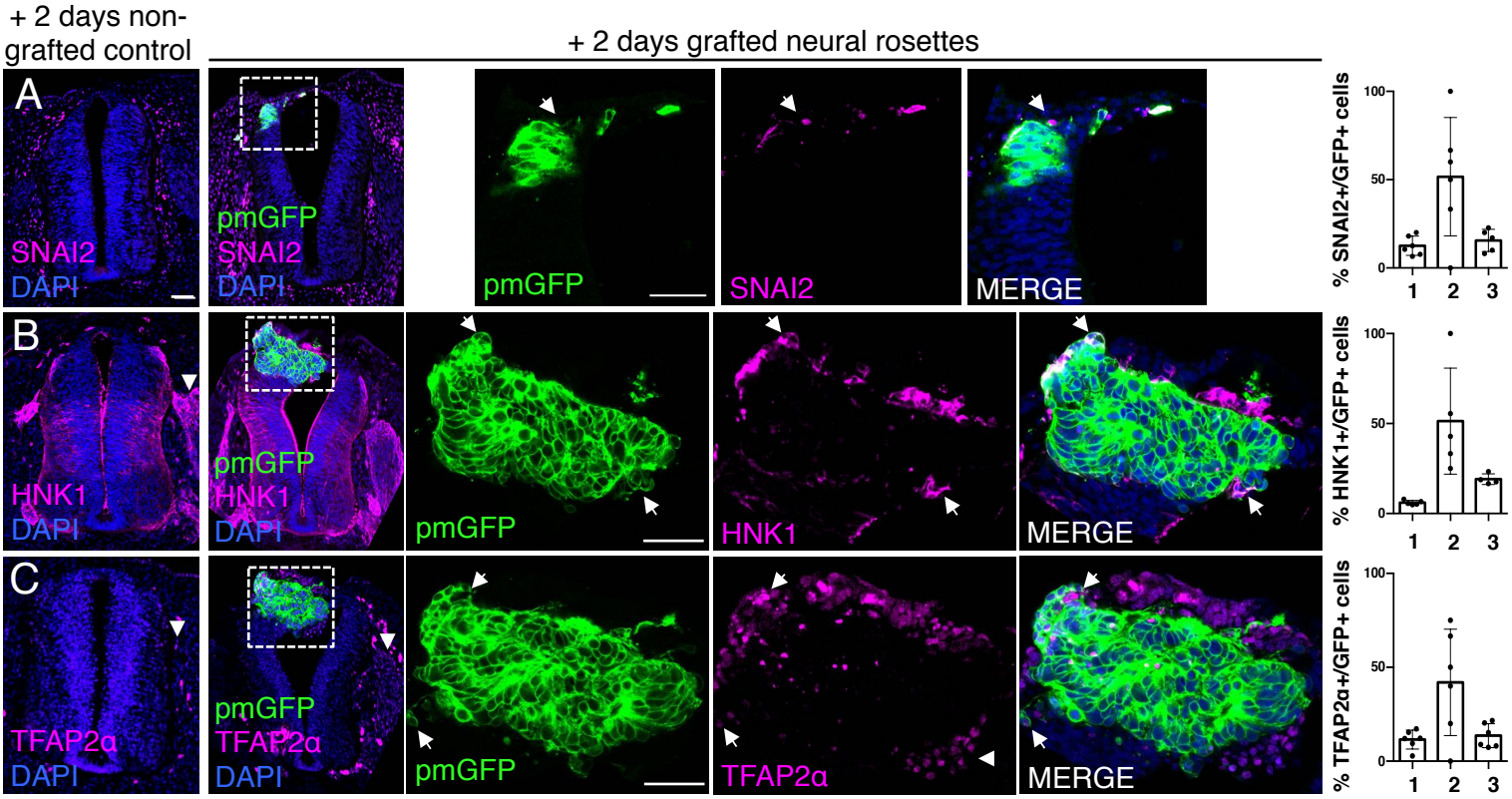

Figure 5. Homo-chronically transplanted hiPSC-derived neural rosettes exhibit cell autonomous neural crest differentiation in the chicken embryonic environment (**A-C**) IF to detect key neural crest marker proteins in control (non-grafted) and grafted embryos after 2 days incubation (**A**) SNAIL2, (**B**) HNK1, (**C**) TFAP2α (arrowheads indicate examples of candidate protein expressing cells in the chicken host tissue; arrows indicate examples of candidate protein and GFP co-expressing cells, note most cells at graft periphery, dashed white boxes indicate area of magnification in next adjacent image). Three transverse sections from each of at least three grafted chicken embryos were analyzed for each marker and the proportions of SNAIL2/GFP +ve, HNK1/GFP +ve and TFAP2α /GFP +ve cells in cell configurations 1, 2 or 3 were quantified, each dot represents an histological section analyzed, note the small number of isolated cells (group 2) underlies lack of significant difference between groups (see Materials and Methods), data analyzed with Mann-Whitney U test. Errors bars are ± SD. Scale bar = 50µm.

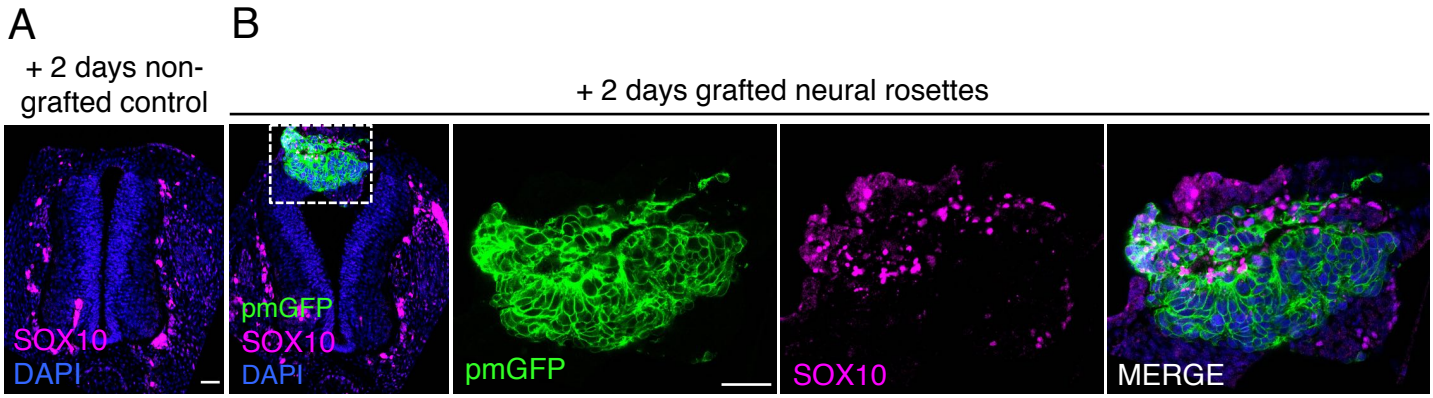

Figure S4. Transplanted human dorsal spinal cord rosettes express SOX10, a specific marker of differentiated neural crest 2 days after grafting. IF to detect expression of the neural crest marker **(A)** SOX10 in control sham operated, and **(B)** grafted chicken embryo following 2 days incubation (dashed white box indicates area of magnification in next adjacent image). One chicken embryo and three sections were analysed. Scale bar = 50µm.

603 Moreover, no ISLET-1 positive cells were found in single cells. This reinforces the conclusion
604 that the pace of human neural differentiation in these rosettes is directed by cell intrinsic
605 factors.

606 Analysis of neural crest differentiation in grafted rosettes after 2 days further
607 confirmed the asynchrony between graft and host cell differentiation progression. SNAI2-
608 expressing neural crest cells where still found within grafted rosettes, while delamination of
609 host neural crest was now complete, as indicated by absence of Snail2 positive cells in the
610 chicken dorsal neural tube (Fig. 5A). Moreover, expression of migratory neural crest markers
611 HNK1 and TFAP2α in the rosette periphery further aligned human rosette differentiation in
612 vivo with that observed in vitro (Figs. 5B, C and S2). As single cells, integrated human cells
613 were more likely to express markers of migrating neural crest cells HNK1 (Fig. 5B) and TFAP2α
614 (Fig. 5C) exhibiting neural crest differentiation progression similar to that found in *in vitro*
615 conditions (Fig. S2).

616 Intriguingly, despite this apparent lack of influence of the chick host on grafted
617 human cells, we found some evidence that human cells altered chick neural crest
618 differentiation. At this stage, chicken neural crest cells have normally delaminated and
619 migrated to the dorsal root ganglia (DRGs) (Kalcheim 1999). However, close to integrated
620 human cells chicken neural crest expressed early migration phase markers HNK1 (Fig. 5B),
621 TFAP2α (Fig. 5C) and Sox10 (Fig. S4) suggesting that the presence of human cells delays
622 progression of the host neural crest differentiation program.

623 Together these findings indicate that after two days, differentiation in grafted human
624 spinal cord rosettes progresses at the same pace as in vitro despite exposure to the more
625 rapidly differentiating environment of the chicken host embryo.

626

627 Longer term analysis reveals impaired differentiation in grafted human neural
628 rosettes

629 To address whether the differentiation pace and trajectory in grafted human rosettes
630 continues in synchrony with that in vitro, analysis was further undertaken five days after
631 grafting. At this time point all human cells were incorporated within the host
632 neuroepithelium, either as cell groups or single cells (Figs. 6A-6B') and the majority of cells
633 remained dorsal neural progenitors expressing SOX2 and PAX7 (Figs. 6C,D). Importantly,
634 neuronal differentiation now continued (Fig. 6E-G) indicated by the increase of P27 and
635 ISLET1 positive human cells. However, the proportion of cells expressing P27 in transplanted
636 rosettes decreased between day 2 and day 5 and was also significantly reduced compared

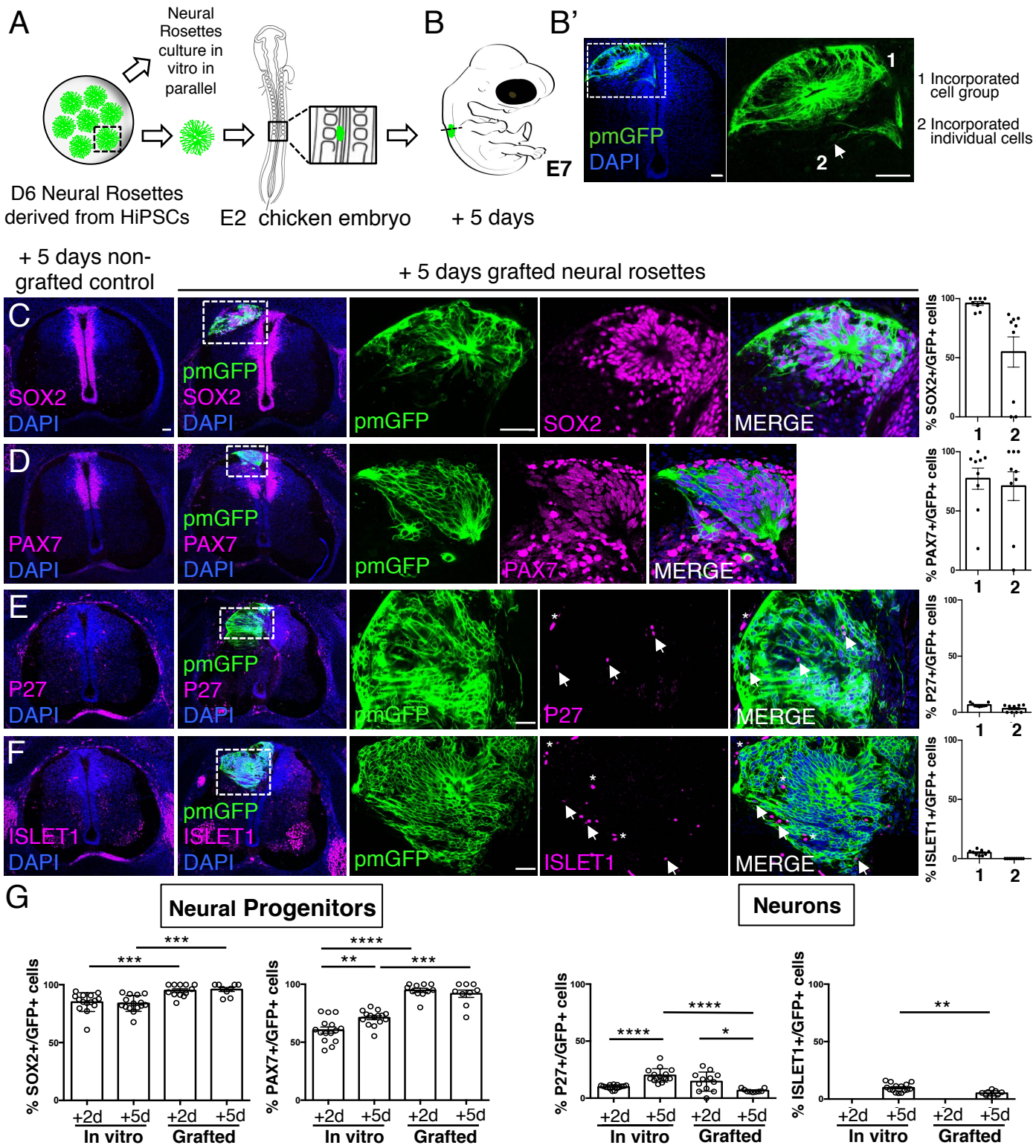

Figure 6. Longer term analysis reveals impaired neuronal differentiation and cell type specification in grafted human neural rosettes (**A**) Schematic of human dorsal spinal cord neural rosette transplantation protocol and (**B-B'**) transplanted cell configurations 5 days after transplantation; (**C-F**) IF to detect key marker proteins in control (non-grafted) and grafted chicken embryos after 5 days incubation, neural progenitor markers (**C**) SOX2, and (**D**) PAX7, post-mitotic neuronal (**E**) P27 and dorsal interneuron type 3, dI3s, (**F**) ISLET1 markers (arrows indicate examples of P27 and GFP co-expressing cells, dashed white boxes indicate area of magnification in next adjacent image, asterisks indicate examples of host blood cells). Three transverse sections from each of at least three grafted chicken embryos were analyzed for each marker and the proportions of SOX2/GFP +ve, PAX7/GFP +ve, P27 /GFP +ve and ISLET1/GFP +ve cells in configurations 1 or 2 were quantified, each dot represents an histological section analyzed, no significant differences were found; (**G**) Comparison of proportion of ChiPS4-pmGFP derived neural progenitors and neurons expressing SOX2, PAX7, P27 and ISLET1 in rosettes cultured in vitro in parallel with those transplanted into chicken embryos, assessed after 2 and 5 days, each dot represents a single rosette (5 rosettes sampled from each to 3 independent differentiations), see Fig S2 and proportions of these same marker proteins in transplanted rosettes after 2 and 5 days in chicken embryonic environment, each dot represents data from one section, with 3 sections from each of 3 grafted chick embryos, analysis Mann-Whitney U test. Errors bars are ± SD. p values (see methods). Scale bar = 50µm.

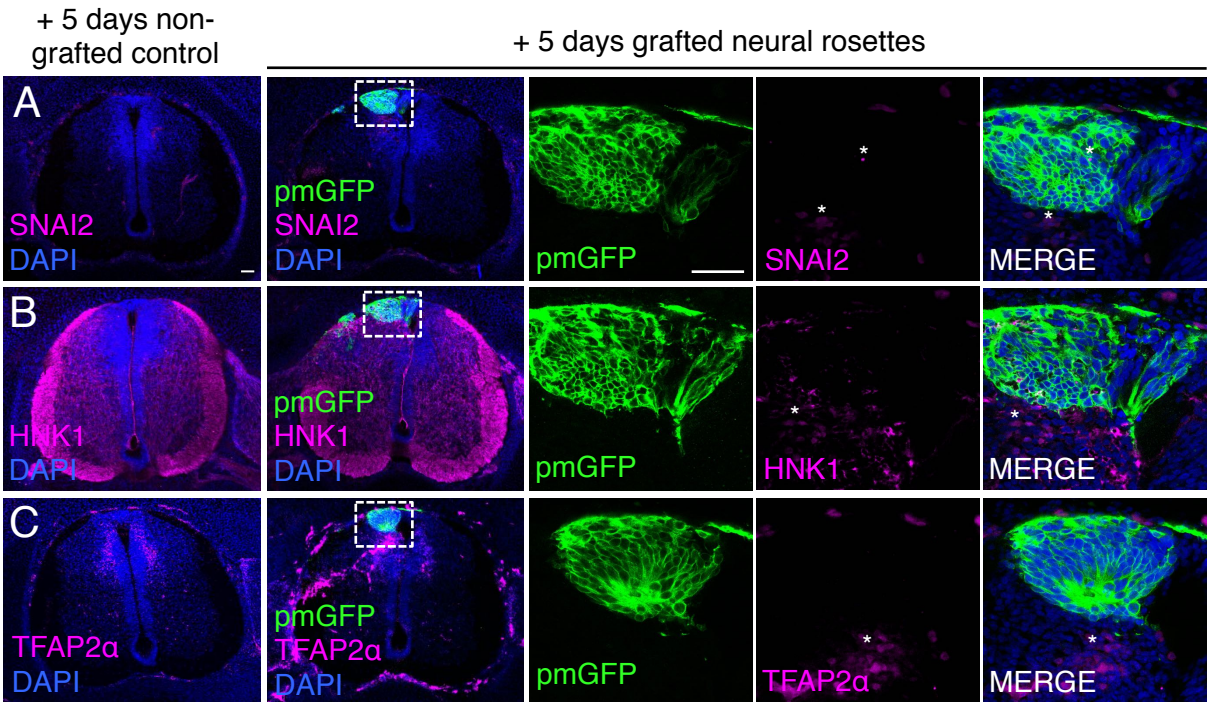

Figure 7. Longer term analysis reveals no neural crest differentiation in grafted human neural rosettes (**A-C**) IF to detect key neural crest marker proteins in control (non-grafted) and grafted chicken embryos after 5 days incubation reveals no expression of neural crest progenitor markers in any cell configurations (**A**) SNAI2 (1: 0/860 GFP+ cells and 2: 0/70 GFP+ cells), (**B**) differentiated neural crest cells HNK1 (1: 0/956 GFP+ cells and 2: 0/57 GFP+ cells) and (**C**) TFAP2α (1: 0/1175 GFP+ cells and 2: 0/66 GFP+ cells) (asterisks indicate host blood cells). At least three chicken embryos and three cross-sections were analyzed for each marker. Scale bar = 50µm.

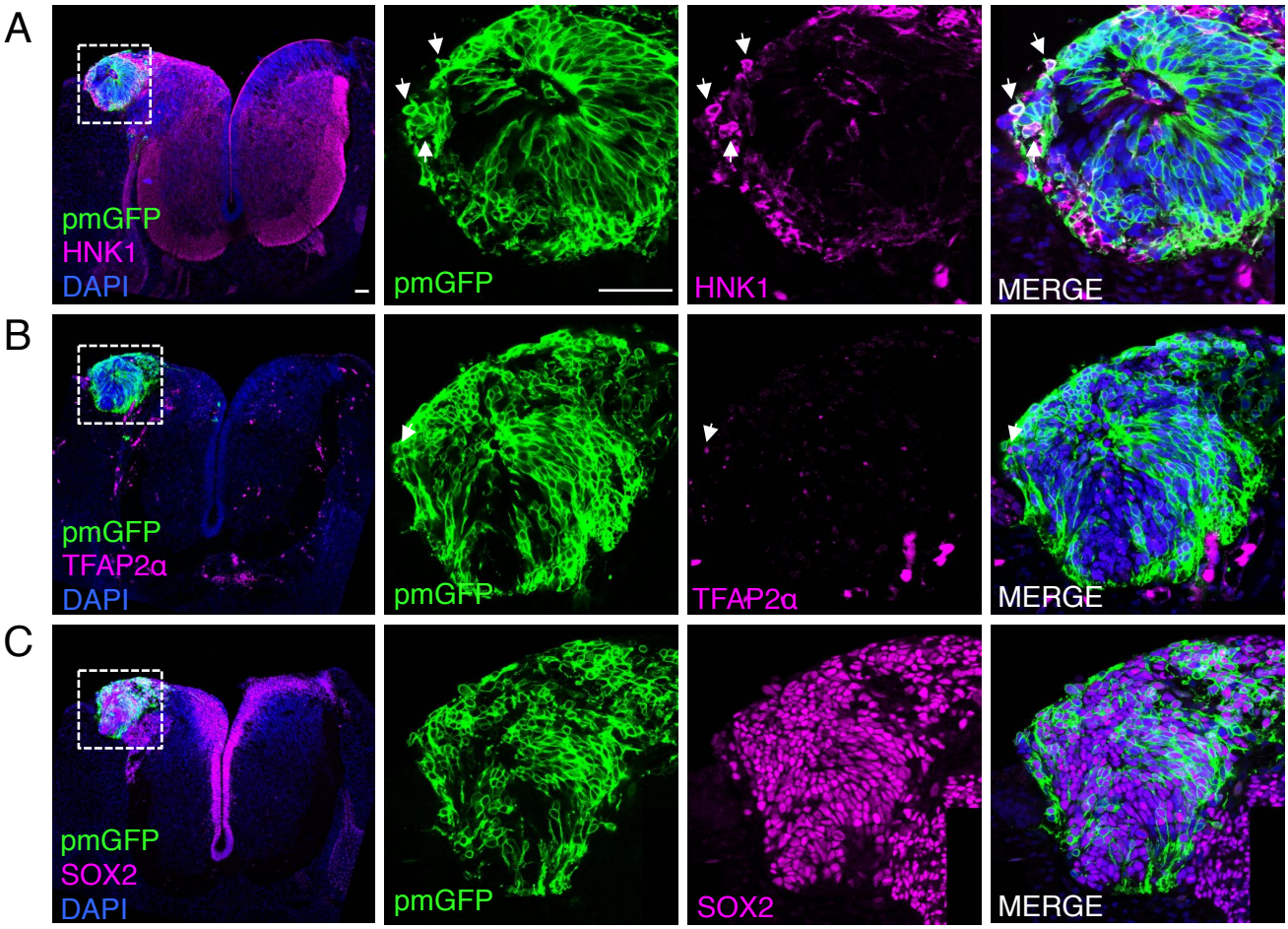

Figure S5. Ectopically positioned human dorsal spinal cord rosette reveals retention of ability to differentiate into neural crest Chicken open neural tube with a human dorsal spinal cord rosette following transplantation 5 days previously, analysed with IF to detect expression of differentiated neural crest cell markers (**A)** HNK1, **(B)** TFAP2α and (**C)** pan-neural marker SOX2 (arrows indicate examples of candidate proteins and GFP co-expressing cells, dashed white boxes indicate area of magnification in next adjacent image). One chicken embryo and three sections were analysed. Scale bar = 50μm.

738 with their in vitro counterparts, where the proportion of P27 cells increased in this time
739 frame (Fig. 6G). The neural marker ISLET1 was first detected five days after grafting, both in
740 vivo and in vitro (equivalent to D11 rosettes) (Fig. 6G, S2). However, the rate of ISLET1
741 positive cells was significantly reduced in transplanted rosettes compared with their in vitro
742 counterparts (Fig. 6G). Moreover, the neural progenitor cell population continued to expand
743 in vivo to greater extent than in vitro, as indicated by higher proportion of SOX2 and PAX7
744 expressing cells in transplanted rosettes (Figs. 6G, S2). Together, these results indicate that,
745 the rate of neurogenesis gradually attenuates in transplanted rosettes while the neural
746 progenitor population expands.

747 Furthermore, day 5 transplanted rosettes lacked the neural crest markers assessed
748 (SNAI2, HNK1 and TFAP2α), but these were detected in rosettes cultured in parallel in vitro
749 (Figs. 7A, B, C and S2). This indicates that this later chicken embryo environment is no longer
750 conducive to human neural crest differentiation. However, we note that human neural crest
751 cells were still generated in one chimera excluded due to open neural tube defects (Fig. S5),
752 suggesting that human neural rosettes retain the potential for such differentiation in an
753 appropriate environment.

754 Overall, longer term analysis of differentiation in transplanted human rosettes
755 revealed that rather than proceeding more rapidly in the chicken embryo, even the intrinsic
756 differentiation pace and trajectories of human dorsal neural progenitors and neural crest are
757 ultimately not sustained and cells in the human rosettes stall in the expansive neural
758 progenitor phase.

759

760 ## Discussion

761 This study presents a novel in vitro human neural rosette assay that recapitulates the
762 temporal sequence of dorsal spinal cord differentiation observed in vertebrate embryos.
763 Importantly, this differentiation programme progresses more rapidly in vitro than in the
764 human embryonic spinal cord. It may therefore capture the cell intrinsic differentiation pace
765 of this cell population, while lacking signals present in the embryo that influence the normal
766 duration of steps in spinal cord differentiation. The initial retention of this in vitro
767 differentiation pace in rosettes challenged by transplantation into the faster differentiating
768 environment of the chicken embryonic spinal cord, further suggests that this reflects a cell
769 intrinsic species-specific differentiation pace. However, analysis of transplanted rosettes after
770 a longer period revealed that not only do these cells fail to respond to differentiation cues in

771 the chick embryonic environment, but also no longer follow their intrinsic differentiation
772 programme, and persist instead in the expansive neural progenitor cell state.
773
774 In vitro differentiation of human pluripotent cell derived neuromesodermal
775 progenitors in minimal medium containing low level retinoic acid (Verrier et al. 2018) was
776 sufficient to generate self-organizing dorsal spinal cord rosettes composed of neural crest and
777 neural progenitors. We demonstrated that such structures reproducibly differentiate in a
778 specific temporal sequence which follows that observed in the embryonic dorsal spinal cord
779 (Fig. 3I), with neural crest differentiating first, then dorsal-interneurons (dI1/3/5s) and finally
780 glial cells (Duband, Dady, and Fleury 2015, Jiang et al. 2009, Andrews et al. 2017, Deneen et
781 al. 2006). One peculiarity in this assay, the lack of dI2/4s interneurons, may be explained by a
782 requirement for more nuanced exposure to BMPs (Andrews et al. 2017, Gupta et al. 2018,
783 Duval et al. 2019), which, although endogenously expressed in this assay, are not exogenously
784 provided in this protocol (Verrier et al. 2018).
785
786 Two lines of evidence indicate that these human dorsal spinal cord rosettes exhibit a
787 cell intrinsic differentiation pace. First, the timing of neural progenitor differentiation was
788 found to be more rapid in vitro than in the human embryo. This was indicated by the earlier
789 appearance of ISLET1+/HB9- expressing neurons and of NFIA expressing gliogenic progenitors
790 in neural rosettes than in the human embryonic dorsal spinal cord; indeed, the period from
791 migratory neural crest emergence to gliogenesis onset was ~1.5 weeks faster in vitro than in
792 the human embryo (Fig 3I). This detailed comparison of the timing of the appearance of
793 specific cell types in the human embryo with in vitro data may help to inform modelling
794 approaches which largely rely on morphological changes to align differentiation tempo
795 (Workman et al. 2013). This discrepancy in differentiation timing supports the idea that in
796 vitro conditions represent a differentiation pace that reflects cell intrinsic constraints.
797 Secondly, homo-chronic transplantation of these rosettes into the chicken neural tube, which
798 has a more rapidly progressing differentiation tempo, did not accelerate rosette
799 differentiation (even in individual human cells incorporated within the chicken
800 neuroepithelium), further suggesting that rosette differentiation pace reflects species-specific
801 cell intrinsic constraints. This conclusion is consistent with the distinct differentiation pace
802 manifest in vitro in human and in mouse ventral neural progenitors cultured in similar
803 conditions, which have been shown to reflect species-specific differences in cell cycle length
804 and general protein stability (Rayon et al. 2020).

805 In this context, it is informative that our experiments demonstrate that the pace of
806 human neural differentiation in vitro is faster than that observed in the human embryo. This
807 likely reflects longer time spent in expansive neural progenitor phases in the embryo, where
808 this leads to generation of a much larger structure than a rosette. This raises the interesting
809 possibility that overall differentiation pace, beyond that governed by cell intrinsic factors,
810 might be influenced by and scale with the size of a self-organising cell group. In vertebrate
811 embryos, however, the timing of specific phases of neural differentiation is known to be
812 orchestrated by signals from adjacent tissues, which drive and coordinate axial
813 differentiation: this includes adjacent somites (Diez del Corral, Breitkreuz, and Storey 2002,
814 Diez del Corral et al. 2003), underlying notochord (Placzek et al. 1990) and overlying
815 ectoderm/roof plate (Liem, Tremml, and Jessell 1997, Lee, Dietrich, and Jessell 2000). Clearly,
816 the localised and temporally controlled characteristics of such regulatory influences are
817 lacking this in vitro assay. The importance of timely exposure to extrinsic cues is further
818 underscored by the cell intrinsic behaviour of transplanted human rosette cells, despite
819 exposure to signals from an appropriate extra-cellular environment. One possibility is that the
820 slower human cell cycle (Rayon et al. 2020) contributes to this lack of response to
821 endogenous chick differentiation cues. Indeed, transcriptional onset of differentiation genes
822 may require exposure to signals in a specific cell cycle phase (Pauklin and Vallier 2013, Pauklin
823 et al. 2016) and involve defined changes in replication timing at the early G1 timing decision
824 point (Dimitrova and Gilbert 1999, Hiratani et al. 2008). Perhaps related to this is the finding
825 that while human and mouse neural progenitor cells similarly transduce exogenously
826 provided signalling molecule sonic hedgehog, human cells are slower to transcribe *OLIG2* and
827 *NKX6.1*, key downstream ventral patterning genes (Rayon et al. 2020).
828
829 Previous studies have used xenografting assays to evaluate the behaviour of human
830 progenitors generated *in vitro* (Valensi-Kurtz et al. 2010, Frith et al. 2018) or for potential
831 long-term regenerative therapy purposes using either neural progenitor cells or differentiated
832 neurons, e.g. (Kumamaru et al. 2018, Kumamaru et al. 2019, Linaro et al. 2019). Here we have
833 focused on the differentiation potential of human neural progenitors in an ectopic cellular
834 environment. We have found that these cells only initially follow the intrinsic differentiation
835 programme that they exhibit in vitro. Five days following rosette transplantation neuronal
836 differentiation declines compared to in vitro conditions, neural crest differentiation ceases
837 and cells retain dorsal neural progenitor gene expression. This loss of differentiation
838 progression reveals a limitation of the cell intrinsic neural differentiation programme and
839 underscores the requirement for appropriate extrinsic inputs to maintain differentiation

840 trajectory. Indeed, this suggests that differentiation signals are soon lacking in the chick
841 embryonic environment but are provisioned sufficiently in minimal culture conditions: this
842 might include exogenously provided retinoic acid. In addition, we cannot rule out inhibitory
843 signals acting on grafted human neural cells. Most striking was the continued expansion of
844 these no longer differentiating transplanted neuroepithelial cells; a behaviour reminiscent of
845 neural cancers such as Glioblastoma that share a similar neural progenitor gene expression
846 profile (Agnihotri et al. 2013, Hassn Mesrati et al. 2020). In addition to providing novel insight
847 into the regulation of human neural differentiation, this assay may therefore also offer an
848 opportunity to study cancer origins as well as inform cell-based therapeutic approaches to
849 neural injury and disease.

Materials and Methods

hESC and hiPSCs culture and differentiation

hESC (H9 or AI03e-DCX-YFP H1 line) and hiPSCs (ChIPS4, Cellartis AB) were maintained as feeder-free cultures in DEF-based medium supplemented with bFGF (30ng/mL, Peprotech, Cat. No. 100-18B) and Noggin (10ng/ml, Peprotech, Cat. No. 120-10C) on Geltrex matrix coated plates (10µg/cm^2, Life Technologies, Cat. No. A1413302), and enzymatically passaged using TryPLselect (Thermofisher, Cat. No. 12563011). For PSC passaging, the medium was complemented by addition of the Rho kinase inhibitor Y-27632 (10mM, Tocris, Cat. No. 1254). HPSC quality control and passage number information are provided as metadata.

For differentiation assays, PSC were plated on Geltrex matrix at 40000cells/cm^2 and shifted to N2B27 medium after 24h. Cells were then differentiated for 3 days (D) in N2B27 supplemented with 3 µM Chiron99021 (Tocris, Cat. No. 4953) and 20ng/ml bFGF (PeproTech, Cat. No. 100-18B), in the presence of 50ng/mL Noggin (Peprotech, Cat. No. 120-10C) and 10ng/mL SB431542 (Tocris, Cat. No. 1614) from D2 to D4 to generate NMPs, see (Verrier et al. 2018). For further differentiation, NMPs were passaged using PBS-EDTA 0.5mM and seeded back at controlled density (10^5 cells/cm^2) on Geltrex (20µg/cm^2, Life Technologies, Cat. No. A1413302) in the presence of Y-27632 (10mM, Tocris, Cat. No. 1254). Cells were then cultured in N2B27 containing 100nM all-trans-Retinoic Acid (SIGMA, Cat. No. R2625) for the indicated time to obtain and differentiate neural progenitors. First human neural rosettes were observed from D06 with this regime. All work with hESCs was undertaken in accordance with the UK Stem Cell Bank steering committee (license numbers SCSC14-28 and SCSC14-29).

Immunofluorescence

Primary antibodies for immunofluorescence were obtained commercially for SOX2 (1/200; Millipore), ZO1 (1/500; Invitrogen), NCAD (1/500; SIGMA), TUJ1 (1/1000; SIGMA (Rabbit) or BioLegend (Mouse), OLIG2 (1/200; Millipore), LHX2 (1/200, SIGMA), TLX3 (1/200, Abcam), ISLET-1 (1/200; Abcam), HB9 (1/10; DHSB), PAX7 (1/10; DHSB), SNAI2 (1/200; BD Biosciences), SOX10 (1/200; BD Biosciences), TFAPα (1/10, Santa Cruz), HNK1 (1/10; DHSB), P27 (1/100, BD Biosciences). Human embryonic tissue fixed in 4% PFA for 2h at 4°C was provided by HDBR tissue bank (project no 200407) and processed for cryo-sectioning using standard procedures. hESCs or iPSCs were fixed in 1% Paraformaldehyde solution overnight at 4°C, permeabilized with 0.1% Trixton X-100 in PBS 1X, subjected to immunofluorescence labeling using appropriate secondary antibodies conjugated to Alexa-fluor 488, 568 or 594 (Life

884 Technologies), and processed for DAPI staining to visualize cell nuclei. Fluorescent images
885 were captured using a Leica SP8 confocal using a 20X air or 63X NA1.2 APO water immersion
886 objectives.

887 Pm-eGFP Plasmid construction for engineering hIPS cells

888 A plasmid was constructed for engineering hIPSCs with the piggybac transposase system
889 using the aPX1 transposon plasmid (kind gift from Timothy Sanders, University of Chicago),
890 containing the cytomegalovirus (CMV) enhancer, chicken b-actin (CAG) promoter expression
891 and including the Invitrogen Gateway RfA cassette, allowing for phiC31-mediated
892 recombination from Gateway Entry vectors. Finally, the CAG promoter and Gateway cassette
893 (cargo) are flanked by two Inverted Terminal Repeat sequences (ITR, TTAA) allowing the
894 piggyback transposon action. To label the cell membrane, a plasma membrane (pm)
895 associated palmitoylated fluorescent protein was generated by the addition of the 20-amino
896 acid sequence of ratGAP-43 MLCCMRRTKQVEKNDEDQKI to the N-terminus of the monomeric
897 enhanced GFP (eGFP) (K. Svoboda, Addgene plasmid 18696) through sequential PCR
898 amplification to make a pm-eGFP sequence. This pm-eGFP sequence was then inserted into
899 the aPX1 donor vector using the Gateway System© (ThermoFisher).
900

901 HiPSCs transfection

902 HiPSCs (Cellartis hIPS4 cell line) cells were transfected using the Neon™ transfection System
903 (Life Technologies, Cat. No. MPK10025). Briefly, a mix of aPX1-pm-eGFP construct and
904 piggyback transposase (Yusa et al. 2011), with a final concentration of 1-2 µg/µl, was added to
905 a solution of 10^7 cells and a single pulse of 1100V with 30 ms duration was delivered via the
906 Neon transfection system©. Transfected cells were then plated back on Geltrex coated dishes
907 (10µg/cm2, Life Technologies) and cultured in DEF-based medium supplemented with bFGF
908 (30ng/mL, Peprotech) and Noggin (10ng/ml, Peprotech).
909

910 Chick embryo grafting assay

911 Fertilized chicken eggs (Gallus gallus domesticus) from a commercial source (Winter Farm,
912 Hertfordshire-Royston, UK) were incubated at 38°C to Hamburger and Hamilton (HH) stage
913 11-12 (13 to 16 somites) (Hamburger 1951). A polyclonal population of transfected hIPS4-pm-
914 eGFP cells were cultured 6 days from NMPs differentiation, newly formed human neural
915 rosettes were then manually micro-dissected using a sharp glass needle (0.290-0.310 mm)
916 (Vitrolife). After resting in CO_2 incubator at 37°C for 2 hours, cell aggregates (diameter ≈ 50-
917 100 µm) were gently dissociated and implanted into the dorsal region of one side of the

918 neural tube of stage HH 11-12 chicken embryos. Before implantation, the dorsal region on
919 one side of the neural tube was removed at the level of the most recently formed somite
920 (Figure S3). Embryos were then harvested 2 days or 5 days post-transplantation (Stage HH 23-
921 24 and HH 30-31 respectively). Chicken embryos were fixed in 4% PFA overnight at 4°C, rinsed
922 in PBS and left in PBS/30% sucrose solution overnight at 4°C, then embedded and in agar,
923 frozen and cryo-sectioned at 20 µm and subjected to immunofluorescence processing (as
924 above).
925
926 Cell counts and statistical analysis
927 At D4 of in vitro differentiation from NMP-like cells, defined fields (200 μm^2) of neural
928 progenitors forming a neural plate-like shape were selected for quantification. At later time
929 points, human neural rosettes were selected for analysis and quantification by their shape
930 (round with a single lumen) and size (neural rosette diameter, D6: 70-100 µm, average: 84
931 µm ± 2,7 µm; D10: 125-137 µm, average: 129 µm ± 1,5 µm; D14: 155-195 µm, average: 179
932 µm ± 2,7 µm). All cell counts are an average percentage of cells positive for each protein of
933 interest compared to total (DAPI+ or GFP+) cells counted within a field of neural progenitors
934 (D4) or a rosette and contacting cells at its periphery. Fifteen fields of neural progenitors (D4)
935 or 15 rosettes (D6 and later) were analysed for each marker (n=15, 5 fields of neural
936 progenitors or rosettes from each of 3 independent differentiation experiments). For
937 transplanted human rosettes at least 3 sections from grafts in 3 different embryos were used
938 to determine the proportion of cells expressing a protein of interest. Transplanted human
939 cells were only counted when cells were positive for GFP, immunoreactivity for protein of
940 interest and DAPI. To avoid counting the same cells in consecutive sections, alternate sections
941 were used for each different immunolabelling assay (4 different immunofluorescent
942 assays/transplanted embryos)(metadata Tables S1-7). Statistical analysis was performed using
943 non-parametric Mann-Whitney U test for none normally distributed data using Prism V8.
944 Results are represented as means +/- SEM or SD as indicated in figures and p-values are
945 indicated with * P<0.05, ** P<0.01, *** P<0.001 and **** P<0.0001.

Acknowledgements

We are grateful to Aida Rodrigo-Albors and to Teresa Rayon and James Briscoe for critical reading of this manuscript. We also thank Dr Boaz Levi (Allen Institute) and WiCell for the hESC H1 line expressing $DCX^{Cit/Y}$. Human embryonic material was provided by the Joint MRC/Wellcome Trust (grant# MR/R006237/1) Human Developmental Biology Resource (www.hdbr.org, project no 200407). This work was supported by a Wellcome Investigator award WT102817AIA and an enhancement award WT102817/Z/13/A to KGS. The confocal microscope used for imaging was purchased with support from Wellcome Trust Multi-User Equipment grant (WT101468).

956 Figure legends

957

958 Figure 1. Human pluripotent cell derivation of NMP-like cells and their
959 differentiation into dorsal spinal cord neural rosettes

960 (A) Timeline and protocol for induction and differentiation of dorsal spinal cord neural rosette
961 from human pluripotent stem cells (hPSC); (B) Expression patterns and quantification of cell
962 type specific proteins in rosettes on days (D)4, D6 and D10 detected by immunofluorescence
963 (IF) combined with DNA stain DAPI: apical polarity marker N-Cadherin (NCAD), neural
964 progenitor markers SOX2, PAX6, early neural crest marker SNAIL2, and dorso-ventrally
965 restricted neural progenitor markers PAX7 and OLIG2. Quantifications indicate proportions of
966 expressing cells in either a defined field on D4 or within a rosette from D6, in 15 samples for
967 each marker (n=5 rosettes from each of 3 independent differentiations, each dot represents a
968 single rosette), see Materials and Methods). Data analysed with Mann-Whitney test, errors
969 bars ± S.E.M, p-values = * $p < 0.05$, ** $p < 0.01$ and **** $p < 0.0001$; Scale bar = 50µm.

970

971 Figure 2. Human dorsal spinal cord rosettes exhibit stereotyped sequence of
972 cell-type specific differentiation

973 (A) Schematic of in vitro sequence of cell-type specific differentiation of dorsal spinal cord
974 rosettes; (B) Emergence of migrating neural crest from rosettes by D10, documented by IF
975 for key marker proteins HNK1, (lumen defined by apical marker ZO-1), SOX10 (neural
976 progenitors defined by SOX2) and TFAP2α and quantified for SOX10 and TFAP2α; (C)
977 Transition from neurogenesis to gliogenesis documented and quantified in immature
978 neuronal reporter line (H1:DCX-YFP) with co-IF for gliogenesis marker Nuclear Factor I-A
979 (NFIA) at key timepoints; (D) P27/KIP1 expression which by analogy identifies most dorsal
980 post-mitotic neurons, confirms neurogenesis onset by D8; (E-G) Emergence of dorsal
981 interneuron (dIs) subtypes by D10 indicated by dI1s/LHX2 (E), dI3s/ISLET1 (F) (note lack of
982 HB9/ ISLET1 co-expression distinguishes these cells from motor neurons) and dI5s/BRN3A.
983 Sample numbers, statistics and error bars as in Figure 1, each dot represents a single rosette
984 and see Materials and Methods; Scale bar = 50µm.

985

986 Figure 3 Characterization of neural progenitors and neuronal subtypes in
987 human embryonic spinal cord and comparison with in vitro neural rosette
988 differentiation

989 (A) CS12 human embryo with anatomical sub-regions indicated and their alignment with in
990 vitro spinal cord rosette differentiation (see text); (B-H) transverse sections through human
991 embryonic spinal cord at sacral, lumbar and thoracic levels at 4/4.5 weeks (CS12/CS13) and at
992 brachial/thoracic at 7/7.5 weeks (CS18) analysed by IF for expression of (B and B') dorsal,
993 PAX7, or ventral, OLIG2, spinal cord progenitor markers (note novel PAX7 detection in the
994 floor plate, arrow) and (B') waning PAX7 at CS18 (arrow); (C) premigratory neural crest cell
995 marker SNAI2 is only detected in sacral regions (arrow) shown here with pan-neural
996 progenitor marker SOX2; (D) differentiating migrating neural crest expressing HNK1 emerges
997 from the lumbar region (arrow); (E) neuronal differentiation detected with pan-neuronal
998 marker TUJ1 is manifest dorsally in lumbar regions; dorsal interneurons indicated by (F) dI1
999 specific transcription factor LHX2 and (G) dI3 identifying ISLET1 expressing cells were not
1000 detected dorsally in any region of the spinal cord at CS12/CS13; (G') dorsal ISLET1
1001 interneurons at CS18; (H, H') gliogenesis marker NFIA detected dorsally only at CS18; (I)
1002 Schematic aligning dorsal brachial/thoracic spinal cord differentiation in human embryo and
1003 in hPSC derived dorsal spinal cord rosettes, based on (1) Bondurand N. et al. 1998, O'Rahilly
1004 and Müller 2007; (2) This study, Rayon T. et al. 2020, Marklund et al 2014; (3) This study,
1005 Rayon T. et al. 2020); three sections were analysed at each level for each marker in n = 2
1006 CS12/13 and n = 1 CS18 human embryos. Scale bar = 50µm.
1007
1008 Figure 4. Homo-chronically transplanted hiPSC-derived neural rosettes exhibit
1009 cell autonomous differentiation despite exposure to more rapidly developing
1010 chicken embryonic environment
1011 (A) Schematic of human dorsal spinal cord neural rosette transplantation experiment; (B-B')
1012 Two days after grafting human cells were observed in: 1) cell groups or 2) isolated individual
1013 cells incorporated within the chicken neural tube, or 3) rosette-like configurations contiguous
1014 with chick neural tube. (C-G) IF to detect key marker proteins in control (note, these non-
1015 grafted /sham operated embryos regenerate the dorsal neural tube by 2 days post-operation)
1016 and grafted embryos after 2 days incubation (C) ZO1, (D) SOX2, (E) PAX7, (F) P27, (G) ISLET1
1017 (arrowheads indicate examples of candidate protein expressing cells in the chicken host
1018 tissue; arrow indicate example of P27 and GFP co-expressing cells, dashed white boxes
1019 indicate area of magnification in next adjacent image), three transverse sections from each of
1020 at least three grafted chicken embryos were analysed for each marker combination and the
1021 proportions of SOX2/GFP +ve, PAX7/GFP +ve and P27/GFP +ve cells in configurations 1, 2 or 3
1022 were quantified, each dot represents data from one histological section, note the small

1023 number of isolated cells (group 2) underlies lack of significant difference between groups (see
1024 Materials and Methods), data analysed with Mann-Whitney U test with. Errors bars are ± SD.
1025 Scale bar = 50µm.
1026
1027 Figure 5. Homo-chronically transplanted hiPSC-derived neural rosettes exhibit
1028 cell autonomous neural crest differentiation in the chicken embryonic
1029 environment
1030 (A-C) IF to detect key neural crest marker proteins in control (non-grafted) and grafted
1031 embryos after 2 days incubation (A) SNAIL2, (B) HNK1, (C) TFAP2α (arrowheads indicate
1032 examples of candidate protein expressing cells in the chicken host tissue; arrows indicate
1033 examples of candidate protein and GFP co-expressing cells, note most cells at graft periphery,
1034 dashed white boxes indicate area of magnification in next adjacent image). Three transverse
1035 sections from each of at least three grafted chicken embryos were analysed for each marker
1036 and the proportions of SNAIL2/GFP +ve, HNK1/GFP +ve and TFAP2α /GFP +ve cells in cell
1037 configurations 1, 2 or 3 were quantified, each dot represents data from one histological
1038 section, note the small number of isolated cells (group 2) underlies lack of significant
1039 difference between groups (see Materials and Methods), data analysed with Mann-Whitney
1040 U test. Errors bars are ± SD. Scale bar = 50µm.
1041
1042 Figure 6. Longer term analysis reveals impaired neuronal differentiation and
1043 cell type specification in grafted human neural rosettes
1044 (A) Schematic of human dorsal spinal cord neural rosette transplantation protocol and (B-B')
1045 transplanted cell configurations 5 days after transplantation; (C-F) IF to detect key marker
1046 proteins in control (non-grafted) and grafted chicken embryos after 5 days incubation, neural
1047 progenitor markers (C) SOX2, and (D) PAX7, post-mitotic neuronal (E) P27 and dorsal
1048 interneuron type 3, dI3s, (F) ISLET1 markers (arrows indicate examples of P27 or ISLET1 and
1049 GFP co-expressing cells, dashed white boxes indicate area of magnification in next adjacent
1050 image, asterisks indicate examples of host blood cells). Three transverse sections from each
1051 of at least three grafted chicken embryos were analysed for each marker and the proportions
1052 of SOX2/GFP +ve, PAX7/GFP +ve, P27 /GFP +ve and ISLET1/GFP +ve cells in configurations 1
1053 or 2 were quantified, each dot represents an histological section analysed, no significant
1054 differences were found; (G) Comparison of proportion of ChiPS4-pmGFP derived neural
1055 progenitors and neurons expressing SOX2, PAX7, P27 and ISLET1 in rosettes cultured in vitro
1056 in parallel with those transplanted into chicken embryos, assessed after 2 and 5 days, each

1057 dot represents a single rosette (5 rosettes sampled from each to 3 independent
1058 differentiations), see Fig S2 and proportions of these same marker proteins in transplanted
1059 rosettes after 2 and 5 days in chicken embryonic environment, each dot represents data from
1060 one section, with 3 sections from each of 3 grafted chick embryos, analysis Mann-Whitney U
1061 test. Errors bars are ± SD. p-values (see Methods). Scale bar = 50µm.
1062
1063 Figure 7. Longer term analysis reveals no neural crest differentiation in
1064 grafted human neural rosettes
1065 (A-C) IF to detect key neural crest marker proteins in control (non-grafted) and grafted
1066 chicken embryos after 5 days incubation reveals no expression of neural crest progenitor
1067 markers in any cell configurations (A) SNAI2 (1: 0/860 GFP+ cells and 2: 0/70 GFP+ cells), (B)
1068 differentiated neural crest cells HNK1 (1: 0/956 GFP+ cells and 2: 0/57 GFP+ cells) and (C)
1069 TFAP2α (1: 0/1175 GFP+ cells and 2: 0/66 GFP+ cells) (asterisks indicate host blood cells). At
1070 least three chicken embryos and three cross-sections were analysed for each marker. Scale
1071 bar = 50µm.

References

Aaku-Saraste, E., A. Hellwig, and W. B. Huttner. 1996. "Loss of occludin and functional tight junctions, but not ZO-1, during neural tube closure--remodeling of the neuroepithelium prior to neurogenesis." *Dev Biol* 180 (2):664-79.

Agnihotri, S., K. E. Burrell, A. Wolf, S. Jalali, C. Hawkins, J. T. Rutka, and G. Zadeh. 2013. "Glioblastoma, a brief review of history, molecular genetics, animal models and novel therapeutic strategies." *Arch Immunol Ther Exp (Warsz)* 61 (1):25-41. doi: 10.1007/s00005-012-0203-0.

Andrews, M. G., L. M. Del Castillo, E. Ochoa-Bolton, K. Yamauchi, J. Smogorzewski, and S. J. Butler. 2017. "BMPs direct sensory interneuron identity in the developing spinal cord using signal-specific not morphogenic activities." *Elife* 6. doi: 10.7554/eLife.30647

Arber, S., B. Han, M. Mendelsohn, M. Smith, T. M. Jessell, and S. Sockanathan. 1999. "Requirement for the homeobox gene Hb9 in the consolidation of motor neuron identity." *Neuron* 23 (4):659-74. doi: 10.1016/s0896-6273(01)80026-x.

Betters, E., Y. Liu, A. Kjaeldgaard, E. Sundstrom, and M. I. Garcia-Castro. 2010. "Analysis of early human neural crest development." *Dev Biol* 344 (2):578-92. doi: 10.1016/j.ydbio.2010.05.012.

Bondurand, N., A. Kobetz, V. Pingault, N. Lemort, F. Encha-Razavi, G. Couly, D. E. Goerich, M. Wegner, M. Abitbol, and M. Goossens. 1998. "Expression of the SOX10 gene during human development." *FEBS Lett* 432 (3):168-72. doi: 10.1016/s0014-5793(98)00843-6.

Bronner-Fraser, M. 1986. "Analysis of the early stages of trunk neural crest migration in avian embryos using monoclonal antibody HNK-1." *Dev Biol* 115 (1):44-55. doi: 10.1016/0012-1606(86)90226-5.

Brown, J. P., S. Couillard-Després, C. M. Cooper-Kuhn, J. Winkler, L. Aigner, and H. G. Kuhn. 2003. "Transient expression of doublecortin during adult neurogenesis." *J Comp Neurol* 467 (1):1-10. doi: 10.1002/cne.10874.

Bylund, M., E. Andersson, B. G. Novitch, and J. Muhr. 2003. "Vertebrate neurogenesis is counteracted by Sox1-3 activity." *Nat Neurosci* 6 (11):1162-8. doi: 10.1038/nn1131.

Catala, M., M. A. Teillet, and N. M. Le Douarin. 1995. "Organization and development of the tail bud analyzed with the quail-chick chimaera system." *Mech Dev* 51 (1):51-65. doi: 10.1016/0925-4773(95)00350-a.

Chiaradia, I., and M. A. Lancaster. 2020. "Brain organoids for the study of human neurobiology at the interface of in vitro and in vivo." *Nat Neurosci*. doi: 10.1038/s41593-020-00730-3.

Dady, A., C. Blavet, and J. L. Duband. 2012. "Timing and kinetics of E- to N-cadherin switch during neurulation in the avian embryo." *Dev Dyn* 241 (8):1333-49. doi: 10.1002/dvdy.23813.

1122 Dady, A., and J. L. Duband. 2017. "Cadherin interplay during neural crest segregation from the
1123 non-neural ectoderm and neural tube in the early chick embryo." *Dev Dyn* 246
1124 (7):550-565. doi: 10.1002/dvdy.24517.
1125
1126 Dady, A., E. Havis, V. Escriou, M. Catala, and J. L. Duband. 2014. "Junctional neurulation: a
1127 unique developmental program shaping a discrete region of the spinal cord highly
1128 susceptible to neural tube defects." *J Neurosci* 34 (39):13208-21. doi:
1129 10.1523/JNEUROSCI.1850-14.2014.
1130
1131 Deneen, B., R. Ho, A. Lukaszewicz, C. J. Hochstim, R. M. Gronostajski, and D. J. Anderson.
1132 2006. "The transcription factor NFIA controls the onset of gliogenesis in the
1133 developing spinal cord." *Neuron* 52 (6):953-68. doi: 10.1016/j.neuron.2006.11.019.
1134
1135 Diez del Corral, R., D. N. Breitkreuz, and K. G. Storey. 2002. "Onset of neuronal differentiation
1136 is regulated by paraxial mesoderm and requires attenuation of FGF signalling."
1137 *Development* 129 (7):1681-91.
1138
1139 Diez del Corral, R., I. Olivera-Martinez, A. Goriely, E. Gale, M. Maden, and K. Storey. 2003.
1140 "Opposing FGF and retinoid pathways control ventral neural pattern, neuronal
1141 differentiation, and segmentation during body axis extension." *Neuron* 40 (1):65-79.
1142 doi: 10.1016/s0896-6273(03)00565-8.
1143
1144 Dimitrova, D. S., and D. M. Gilbert. 1999. "The spatial position and replication timing of
1145 chromosomal domains are both established in early G1 phase." *Mol Cell* 4 (6):983-
1146 93. doi: 10.1016/s1097-2765(00)80227-0.
1147
1148 Duband, J. L., A. Dady, and V. Fleury. 2015. "Resolving time and space constraints during
1149 neural crest formation and delamination." *Curr Top Dev Biol* 111:27-67. doi:
1150 10.1016/bs.ctdb.2014.11.002.
1151
1152 Duval, N., C. Vaslin, T. C. Barata, Y. Frarma, V. Contremoulins, X. Baudin, S. Nedelec, and V. C.
1153 Ribes. 2019. "BMP4 patterns Smad activity and generates stereotyped cell fate
1154 organization in spinal organoids." *Development* 146 (14). doi: 10.1242/dev.175430.
1155
1156 Edri, S., P. Hayward, W. Jawaid, and A. Martinez Arias. 2019. "Neuro-mesodermal progenitors
1157 (NMPs): a comparative study between pluripotent stem cells and embryo-derived
1158 populations." *Development* 146 (12). doi: 10.1242/dev.180190.
1159
1160 Ellis, P., B. M. Fagan, S. T. Magness, S. Hutton, O. Taranova, S. Hayashi, A. McMahon, M. Rao,
1161 and L. Pevny. 2004. "SOX2, a persistent marker for multipotential neural stem cells
1162 derived from embryonic stem cells, the embryo or the adult." *Dev Neurosci* 26 (2-
1163 4):148-65. doi: 10.1159/000082134.
1164
1165 Fedorova, V., T. Vanova, L. Elrefae, J. Pospisil, M. Petrasova, V. Kolajova, Z. Hudacova, J.
1166 Baniariova, M. Barak, L. Peskova, T. Barta, M. Kaucka, M. Killinger, J. Vecera, O.
1167 Bernatik, L. Cajanek, H. Hribkova, and D. Bohaciakova. 2019. "Differentiation of neural
1168 rosettes from human pluripotent stem cells in vitro is sequentially regulated on a
1169 molecular level and accomplished by the mechanism reminiscent of secondary
1170 neurulation." *Stem Cell Res* 40:101563. doi: 10.1016/j.scr.2019.101563.

1171 Fedtsova, N. G., and E. E. Turner. 1995. "Brn-3.0 expression identifies early post-mitotic CNS
1172 neurons and sensory neural precursors." *Mech Dev* 53 (3):291-304. doi:
1173 10.1016/0925-4773(95)00435-1.
1174
1175 Frith, T. J., I. Granata, M. Wind, E. Stout, O. Thompson, K. Neumann, D. Stavish, P. R. Heath, D.
1176 Ortmann, J. O. Hackland, K. Anastassiadis, M. Gouti, J. Briscoe, V. Wilson, S. L.
1177 Johnson, M. Placzek, M. R. Guarracino, P. W. Andrews, and A. Tsakiridis. 2018.
1178 "Human axial progenitors generate trunk neural crest cells in vitro." *Elife* 7. doi:
1179 10.7554/eLife.35786.
1180
1181 Frith, T. J. R., and A. Tsakiridis. 2019. "Efficient Generation of Trunk Neural Crest and
1182 Sympathetic Neurons from Human Pluripotent Stem Cells Via a Neuromesodermal
1183 Axial Progenitor Intermediate." *Curr Protoc Stem Cell Biol* 49 (1):e81. doi:
1184 10.1002/cpsc.81.
1185
1186 Glasgow, S. M., J. C. Carlson, W. Zhu, L. S. Chaboub, P. Kang, H. K. Lee, Y. M. Clovis, B. E. Lozzi,
1187 R. J. McEvilly, M. G. Rosenfeld, C. J. Creighton, S. K. Lee, C. A. Mohila, and B. Deneen.
1188 2017. "Glia-specific enhancers and chromatin structure regulate NFIA expression and
1189 glioma tumorigenesis." *Nat Neurosci* 20 (11):1520-1528. doi: 10.1038/nn.4638.
1190
1191 Gleeson, J. G., P. T. Lin, L. A. Flanagan, and C. A. Walsh. 1999. "Doublecortin is a microtubule-
1192 associated protein and is expressed widely by migrating neurons." *Neuron* 23
1193 (2):257-71. doi: 10.1016/s0896-6273(00)80778-3.
1194
1195 Gouti, M., J. Delile, D. Stamataki, F. J. Wymeersch, Y. Huang, J. Kleinjung, V. Wilson, and J.
1196 Briscoe. 2017. "A Gene Regulatory Network Balances Neural and Mesoderm
1197 Specification during Vertebrate Trunk Development." *Dev Cell* 41 (3):243-261.e7. doi:
1198 10.1016/j.devcel.2017.04.002.
1199
1200 Gouti, M., V. Metzis, and J. Briscoe. 2015. "The route to spinal cord cell types: a tale of signals
1201 and switches." *Trends Genet* 31 (6):282-9. doi: 10.1016/j.tig.2015.03.001.
1202
1203 Gouti, M., A. Tsakiridis, F. J. Wymeersch, Y. Huang, J. Kleinjung, V. Wilson, and J. Briscoe.
1204 2014. "In vitro generation of neuromesodermal progenitors reveals distinct roles for
1205 wnt signalling in the specification of spinal cord and paraxial mesoderm identity."
1206 *PLoS Biol* 12 (8):e1001937. doi: 10.1371/journal.pbio.1001937.
1207
1208 Gruss, P., and C. Walther. 1992. "Pax in development." *Cell* 69 (5):719-22. doi: 10.1016/0092-
1209 8674(92)90281-g.
1210
1211 Gui, H., S. Li, and M. P. Matise. 2007. "A cell-autonomous requirement for Cip/Kip cyclin-
1212 kinase inhibitors in regulating neuronal cell cycle exit but not differentiation in the
1213 developing spinal cord." *Dev Biol* 301 (1):14-26. doi: 10.1016/j.ydbio.2006.10.035.
1214
1215 Gupta, S., D. Sivalingam, S. Hain, C. Makkar, E. Sosa, A. Clark, and S. J. Butler. 2018. "Deriving
1216 Dorsal Spinal Sensory Interneurons from Human Pluripotent Stem Cells." *Stem Cell*
1217 *Reports* 10 (2):390-405. doi: 10.1016/j.stemcr.2017.12.012.
1218
1219 Gurdon, J. B. 1988. "A community effect in animal development." *Nature* 336 (6201):772-4.
1220 doi: 10.1038/336772a0.

1221 Hamburger, V.; Hamilton, H. L. 1951. "A series of normal stages in the development of the
1222 chick embryo." *J morphol* 88.49-92.
1223
1224 Hassn Mesrati, M., A. B. Behrooz, Y. Abuhamad A, and A. Syahir. 2020. "Understanding
1225 Glioblastoma Biomarkers: Knocking a Mountain with a Hammer." *Cells* 9 (5). doi:
1226 10.3390/cells9051236.
1227
1228 Hatta, K., and M. Takeichi. 1986. "Expression of N-cadherin adhesion molecules associated
1229 with early morphogenetic events in chick development." *Nature* 320 (6061):447-9.
1230 doi: 10.1038/320447a0.
1231
1232 Henrique, D., E. Abranches, L. Verrier, and K. G. Storey. 2015. "Neuromesodermal progenitors
1233 and the making of the spinal cord." *Development* 142 (17):2864-75. doi:
1234 10.1242/dev.119768.
1235
1236 Hiratani, I., T. Ryba, M. Itoh, T. Yokochi, M. Schwaiger, C. W. Chang, Y. Lyou, T. M. Townes, D.
1237 Schübeler, and D. M. Gilbert. 2008. "Global reorganization of replication domains
1238 during embryonic stem cell differentiation." *PLoS Biol* 6 (10):e245. doi:
1239 10.1371/journal.pbio.0060245.
1240
1241 Hubaud, A., and O. Pourquié. 2014. "Signalling dynamics in vertebrate segmentation." *Nat*
1242 *Rev Mol Cell Biol* 15 (11):709-21. doi: 10.1038/nrm3891.
1243
1244 Jiang, X., Y. Gwye, S. J. McKeown, M. Bronner-Fraser, C. Lutzko, and E. R. Lawlor. 2009.
1245 "Isolation and characterization of neural crest stem cells derived from in vitro-
1246 differentiated human embryonic stem cells." *Stem Cells Dev* 18 (7):1059-70. doi:
1247 10.1089/scd.2008.0362.
1248
1249 Jostes, B., C. Walther, and P. Gruss. 1990. "The murine paired box gene, Pax7, is expressed
1250 specifically during the development of the nervous and muscular system." *Mech Dev*
1251 33 (1):27-37. doi: 10.1016/0925-4773(90)90132-6.
1252 Kalcheim, Le Douarin and. 1999. The neural crest.
1253
1254 Kumamaru, H., K. Kadoya, A. F. Adler, Y. Takashima, L. Graham, G. Coppola, and M. H.
1255 Tuszynski. 2018. "Generation and post-injury integration of human spinal cord neural
1256 stem cells." *Nat Methods* 15 (9):723-731. doi: 10.1038/s41592-018-0074-3.
1257
1258 Kumamaru, H., P. Lu, E. S. Rosenzweig, K. Kadoya, and M. H. Tuszynski. 2019. "Regenerating
1259 Corticospinal Axons Innervate Phenotypically Appropriate Neurons within Neural
1260 Stem Cell Grafts." *Cell Rep* 26 (9):2329-2339.e4. doi: 10.1016/j.celrep.2019.01.099.
1261
1262 Lai, H. C., R. P. Seal, and J. E. Johnson. 2016. "Making sense out of spinal cord somatosensory
1263 development." *Development* 143 (19):3434-3448. doi: 10.1242/dev.139592.
1264
1265 Lancaster, M. A., M. Renner, C. A. Martin, D. Wenzel, L. S. Bicknell, M. E. Hurles, T. Homfray, J.
1266 M. Penninger, A. P. Jackson, and J. A. Knoblich. 2013. "Cerebral organoids model
1267 human brain development and microcephaly." *Nature* 501 (7467):373-9. doi:
1268 10.1038/nature12517.
1269

Lee, K. J., P. Dietrich, and T. M. Jessell. 2000. "Genetic ablation reveals that the roof plate is essential for dorsal interneuron specification." *Nature* 403 (6771):734-40. doi: 10.1038/35001507.

Liem, K. F., Jr., G. Tremml, and T. M. Jessell. 1997. "A role for the roof plate and its resident TGFbeta-related proteins in neuronal patterning in the dorsal spinal cord." *Cell* 91 (1):127-38. doi: 10.1016/s0092-8674(01)80015-5.

Linaro, D., B. Vermaercke, R. Iwata, A. Ramaswamy, B. Libé-Philippot, L. Boubakar, B. A. Davis, K. Wierda, K. Davie, S. Poovathingal, P. A. Penttila, A. Bilheu, L. De Bruyne, D. Gall, K. K. Conzelmann, V. Bonin, and P. Vanderhaeghen. 2019. "Xenotransplanted Human Cortical Neurons Reveal Species-Specific Development and Functional Integration into Mouse Visual Circuits." *Neuron* 104 (5):972-986.e6. doi: 10.1016/j.neuron.2019.10.002.

Marklund, U., Z. Alekseenko, E. Andersson, S. Falci, M. Westgren, T. Perlmann, A. Graham, E. Sundstrom, and J. Ericson. 2014. "Detailed expression analysis of regulatory genes in the early developing human neural tube." *Stem Cells Dev* 23 (1):5-15. doi: 10.1089/scd.2013.0309.

Matsuda, M., Y. Yamanaka, M. Uemura, M. Osawa, M. K. Saito, A. Nagahashi, M. Nishio, L. Guo, S. Ikegawa, S. Sakurai, S. Kihara, T. L. Maurissen, M. Nakamura, T. Matsumoto, H. Yoshitomi, M. Ikeya, N. Kawakami, T. Yamamoto, K. Woltjen, M. Ebisuya, J. Toguchida, and C. Alev. 2020. "Recapitulating the human segmentation clock with pluripotent stem cells." *Nature* 580 (7801):124-129. doi: 10.1038/s41586-020-2144-9.

Meinhardt, A., D. Eberle, A. Tazaki, A. Ranga, M. Niesche, M. Wilsch-Bräuninger, A. Stec, G. Schackert, M. Lutolf, and E. M. Tanaka. 2014. "3D reconstitution of the patterned neural tube from embryonic stem cells." *Stem Cell Reports* 3 (6):987-99. doi: 10.1016/j.stemcr.2014.09.020.

Menezes, J. R., and M. B. Luskin. 1994. "Expression of neuron-specific tubulin defines a novel population in the proliferative layers of the developing telencephalon." *J Neurosci* 14 (9):5399-416.

Mizuguchi, R., M. Sugimori, H. Takebayashi, H. Kosako, M. Nagao, S. Yoshida, Y. Nabeshima, K. Shimamura, and M. Nakafuku. 2001. "Combinatorial roles of olig2 and neurogenin2 in the coordinated induction of pan-neuronal and subtype-specific properties of motoneurons." *Neuron* 31 (5):757-71. doi: 10.1016/s0896-6273(01)00413-5.

Moris, N., K. Anlas, S. C. van den Brink, A. Alemany, J. Schröder, S. Ghimire, T. Balayo, A. van Oudenaarden, and A. Martinez Arias. 2020. "An in vitro model of early anteroposterior organization during human development." *Nature* 582 (7812):410-415. doi: 10.1038/s41586-020-2383-9.

Namba, T., J. Dóczi, A. Pinson, L. Xing, N. Kalebic, M. Wilsch-Bräuninger, K. R. Long, S. Vaid, J. Lauer, A. Bogdanova, B. Borgonovo, A. Shevchenko, P. Keller, D. Drechsel, T. Kurzchalia, P. Wimberger, C. Chinopoulos, and W. B. Huttner. 2020. "Human-Specific ARHGAP11B Acts in Mitochondria to Expand Neocortical Progenitors by Glutaminolysis." *Neuron* 105 (5):867-881.e9. doi: 10.1016/j.neuron.2019.11.027.

1321 Nieto, M. A. 2002. "The snail superfamily of zinc-finger transcription factors." *Nat Rev Mol*
1322 *Cell Biol* 3 (3):155-66. doi: 10.1038/nrm757.
1323
1324 Ninkina, N. N., G. E. Stevens, J. N. Wood, and W. D. Richardson. 1993. "A novel Brn3-like POU
1325 transcription factor expressed in subsets of rat sensory and spinal cord neurons."
1326 *Nucleic Acids Res* 21 (14):3175-82. doi: 10.1093/nar/21.14.3175.
1327
1328 Novitch, B. G., A. I. Chen, and T. M. Jessell. 2001. "Coordinate regulation of motor neuron
1329 subtype identity and pan-neuronal properties by the bHLH repressor Olig2." *Neuron*
1330 31 (5):773-89. doi: 10.1016/s0896-6273(01)00407-x.
1331
1332 O'Rahilly, R. 1987. "Human embryo." *Nature* 329 (6138):385. doi: 10.1038/329385e0.
1333
1334 O'Rahilly, R., and F. Muller. 2007. "The development of the neural crest in the human." *J Anat*
1335 211 (3):335-51. doi: 10.1111/j.1469-7580.2007.00773.x.
1336
1337 Ogura, Takenori, Hideya Sakaguchi, Susumu Miyamoto, and Jun Takahashi. 2018. "Three-
1338 dimensional induction of dorsal, intermediate and ventral spinal cord tissues from
1339 human pluripotent stem cells." *Development* 145 (16):dev162214. doi:
1340 10.1242/dev.162214.
1341
1342 Otani, T., M. C. Marchetto, F. H. Gage, B. D. Simons, and F. J. Livesey. 2016. "2D and 3D Stem
1343 Cell Models of Primate Cortical Development Identify Species-Specific Differences in
1344 Progenitor Behavior Contributing to Brain Size." *Cell Stem Cell* 18 (4):467-80. doi:
1345 10.1016/j.stem.2016.03.003.
1346
1347 Pauklin, S., P. Madrigal, A. Bertero, and L. Vallier. 2016. "Initiation of stem cell differentiation
1348 involves cell cycle-dependent regulation of developmental genes by Cyclin D." *Genes*
1349 *Dev* 30 (4):421-33. doi: 10.1101/gad.271452.115.
1350
1351 Pauklin, S., and L. Vallier. 2013. "The cell-cycle state of stem cells determines cell fate
1352 propensity." *Cell* 155 (1):135-47. doi: 10.1016/j.cell.2013.08.031.
1353
1354 Pevny, L. H., S. Sockanathan, M. Placzek, and R. Lovell-Badge. 1998. "A role for SOX1 in neural
1355 determination." *Development* 125 (10):1967-78.
1356
1357 Placzek, M., M. Tessier-Lavigne, T. Yamada, T. Jessell, and J. Dodd. 1990. "Mesodermal control
1358 of neural cell identity: floor plate induction by the notochord." *Science* 250
1359 (4983):985-8. doi: 10.1126/science.2237443.
1360
1361 Rayon, T., D. Stamataki, R. Perez-Carrasco, L. Garcia-Perez, C. Barrington, M. Melchionda, K.
1362 Exelby, J. Lazaro, V. L. J. Tybulewicz, E. M. C. Fisher, and J. Briscoe. 2020. "Species-
1363 specific pace of development is associated with differences in protein stability."
1364 *Science* 369 (6510). doi: 10.1126/science.aba7667.
1365
1366 Schoenwolf, G. C., and D. H. Nichols. 1984. "Histological and ultrastructural studies on the
1367 origin of caudal neural crest cells in mouse embryos." *J Comp Neurol* 222 (4):496-
1368 505. doi: 10.1002/cne.902220404.
1369
1370 Sofroniew, M. V. 2018. "Dissecting spinal cord regeneration." *Nature* 557 (7705):343-350.
1371 doi: 10.1038/s41586-018-0068-4.

1372 Steventon, B., and A. Martinez Arias. 2017. "Evo-engineering and the cellular and molecular
1373 origins of the vertebrate spinal cord." *Dev Biol* 432 (1):3-13. doi:
1374 10.1016/j.ydbio.2017.01.021.
1375
1376 Tucker, G. C., H. Aoyama, M. Lipinski, T. Tursz, and J. P. Thiery. 1984. "Identical reactivity of
1377 monoclonal antibodies HNK-1 and NC-1: conservation in vertebrates on cells derived
1378 from the neural primordium and on some leukocytes." *Cell Differ* 14 (3):223-30. doi:
1379 10.1016/0045-6039(84)90049-6.
1380
1381 Turner, D. A., P. C. Hayward, P. Baillie-Johnson, P. Rué, R. Broome, F. Faunes, and A. Martinez
1382 Arias. 2014. "Wnt/β-catenin and FGF signalling direct the specification and
1383 maintenance of a neuromesodermal axial progenitor in ensembles of mouse
1384 embryonic stem cells." *Development* 141 (22):4243-53. doi: 10.1242/dev.112979.
1385
1386 Turnpenny, P. D., B. Alman, A. S. Cornier, P. F. Giampietro, A. Offiah, O. Tassy, O. Pourquié, K.
1387 Kusumi, and S. Dunwoodie. 2007. "Abnormal vertebral segmentation and the notch
1388 signaling pathway in man." *Dev Dyn* 236 (6):1456-74. doi: 10.1002/dvdy.21182.
1389
1390 Tzouanacou, E., A. Wegener, F. J. Wymeersch, V. Wilson, and J. F. Nicolas. 2009. "Redefining
1391 the progression of lineage segregations during mammalian embryogenesis by clonal
1392 analysis." *Dev Cell* 17 (3):365-76. doi: 10.1016/j.devcel.2009.08.002.
1393
1394 Uchikawa, M., Y. Ishida, T. Takemoto, Y. Kamachi, and H. Kondoh. 2003. "Functional analysis
1395 of chicken Sox2 enhancers highlights an array of diverse regulatory elements that are
1396 conserved in mammals." *Dev Cell* 4 (4):509-19. doi: 10.1016/s1534-5807(03)00088-
1397 1.
1398
1399 Uchikawa, M., M. Yoshida, M. Iwafuchi-Doi, K. Matsuda, Y. Ishida, T. Takemoto, and H.
1400 Kondoh. 2011. "B1 and B2 Sox gene expression during neural plate development in
1401 chicken and mouse embryos: universal versus species-dependent features." *Dev*
1402 *Growth Differ* 53 (6):761-71. doi: 10.1111/j.1440-169X.2011.01286.x.
1403
1404 Valensi-Kurtz, M., S. Lefler, M. A. Cohen, M. Aharonowiz, R. Cohen-Kupiec, A. Sheinin, U.
1405 Ashery, B. Reubinoff, and M. Weil. 2010. "Enriched population of PNS neurons
1406 derived from human embryonic stem cells as a platform for studying peripheral
1407 neuropathies." *PLoS One* 5 (2):e9290. doi: 10.1371/journal.pone.0009290.
1408
1409 Verrier, L., L. Davidson, M. Gierlinski, A. Dady, and K. G. Storey. 2018. "Neural differentiation,
1410 selection and transcriptomic profiling of human neuromesodermal progenitor-like
1411 cells in vitro." *Development* 145 (16). doi: 10.1242/dev.166215.
1412
1413 Walther, C., and P. Gruss. 1991. "Pax-6, a murine paired box gene, is expressed in the
1414 developing CNS." *Development* 113 (4):1435-49.
1415
1416 Workman, Alan D., Christine J. Charvet, Barbara Clancy, Richard B. Darlington, and Barbara L.
1417 Finlay. 2013. "Modeling Transformations of Neurodevelopmental Sequences across
1418 Mammalian Species." *The Journal of Neuroscience* 33 (17):7368. doi:
1419 10.1523/JNEUROSCI.5746-12.2013.
1420
1421 Yao, Z., J. K. Mich, S. Ku, V. Menon, A. R. Krostag, R. A. Martinez, L. Furchtgott, H. Mulholland,
1422 S. Bort, M. A. Fuqua, B. W. Gregor, R. D. Hodge, A. Jayabalu, R. C. May, S. Melton, A.

1423 M. Nelson, N. K. Ngo, N. V. Shapovalova, S. I. Shehata, M. W. Smith, L. J. Tait, C. L.
1424 Thompson, E. R. Thomsen, C. Ye, I. A. Glass, A. Kaykas, S. Yao, J. W. Phillips, J. S.
1425 Grimley, B. P. Levi, Y. Wang, and S. Ramanathan. 2017. "A Single-Cell Roadmap of
1426 Lineage Bifurcation in Human ESC Models of Embryonic Brain Development." *Cell*
1427 *Stem Cell* 20 (1):120-134. doi: 10.1016/j.stem.2016.09.011.
1428
1429 Yusa, K., L. Zhou, M. A. Li, A. Bradley, and N. L. Craig. 2011. "A hyperactive piggyBac
1430 transposase for mammalian applications." *Proc Natl Acad Sci U S A* 108 (4):1531-6.
1431 doi: 10.1073/pnas.1008322108.
1432
1433 Zhang, C. L., T. Huang, B. L. Wu, W. X. He, and D. Liu. 2017. "Stem cells in cancer therapy:
1434 opportunities and challenges." *Oncotarget* 8 (43):75756-75766. doi:
1435 10.18632/oncotarget.20798.
1436
1437 Zhang, J., S. Hagopian-Donaldson, G. Serbedzija, J. Elsemore, D. Plehn-Dujowich, A. P.
1438 McMahon, R. A. Flavell, and T. Williams. 1996. "Neural tube, skeletal and body wall
1439 defects in mice lacking transcription factor AP-2." *Nature* 381 (6579):238-41. doi:
1440 10.1038/381238a0.
1441

	D4			D6			D10		
	Positive Cells	Total cells	%	Positive Cells	Total cells	%	Positive Cells	Total cells	%
SOX2	142	206	68.932	60	80	75	171	208	82.211
	150	221	67.873	78	88	88.636	162	195	83.076
	193	237	81.434	67	90	74.444	190	230	82.608
	262	312	83.974	65	96	67.708	155	194	79.896
	139	185	75.135	58	95	61.052	186	202	92.079
	140	195	71.794	81	90	90	136	183	74.316
	320	478	66.945	83	101	82.178	179	200	89.5
	225	325	69.23	95	119	79.831	150	194	77.319
	195	261	74.712	74	82	90.243	185	223	82.959
	150	231	64.935	67	92	72.826	114	138	82.608
	160	210	76.19	65	95	68.421	146	171	85.38
	157	246	63.821	58	80	72.5	106	143	74.125
	281	322	87.267	62	103	60.784	92	124	74.193
	142	193	73.575	67	101	66.336	102	137	74.452
				42	78	53.846	84	113	74.336

	D4	D6	D10
mean	73.27264286	73.587	80.60386667
sd	7.106480884	11.0684337	5.77519715
SEM	1.899286907	2.857857293	1.491149492

n=3 independent differentiations
N=15 field of view at D04 (5 per differentiation)
N=15 rosettes (5 rosettes per differentiation)

	D4			D6			D10		
	Positive Cells	Total cells	%	Positive Cells	Total cells	%	Positive Cells	Total cells	%
PAX6	84	226	37.168	35	65	53.846	48	121	39.669
	55	140	39.285	45	109	41.284	45	119	37.815
	56	144	38.888	48	93	51.612	53	102	51.96
	105	219	47.945	35	90	38.888	55	127	43.307
	30	180	16.666	29	98	29.591	47	125	37.6
	77	208	37.019	44	84	52.38	38	112	33.928
	50	190	26.315	48	93	51.612	31	115	26.956
	50	164	30.487	51	117	43.589	42	105	40
	103	204	50.49	57	120	47.5	39	110	35.454
	58	154	37.662	37	109	33.94	55	130	42.307
	64	150	42.666	55	97	56.701	65	143	45.454
	80	200	40	47	115	40.869	79	161	49.068
	64	190	33.684	45	96	46.875	73	140	52.142
	54	166	32.53	52	125	40.8	51	145	35.172
				58	106	54.716	57	151	37.748

	D4	D6	D10
mean	36.48607143	45.61353333	40.572
sd	8.546111437	8.032117234	6.97188923
SEM	2.284044356	2.073883752	1.800134058

	D4			D6			D10		
	Positive Cells	Total cells	%	Positive Cells	Total cells	%	Positive Cells	Total cells	%
SNAI2	80	322	24.844	41	103	39.805	30	208	14.423
	40	193	20.725	36	101	35.643	26	195	13.333
	30	131	22.9	23	78	29.487	36	230	15.652
	41	206	19.902	28	107	26.168	28	194	14.432
	58	279	20.788	31	95	32.631	18	202	8.91
	62	312	18.871	28	106	26.415	37	183	20.218
	70	259	27.027	33	101	32.673	29	200	14.5
	37	245	15.102	34	123	27.642	35	194	18.041
	44	222	19.819	36	85	42.352	30	223	13.452
	45	210	21.428	37	95	35.789	33	138	23.913
	72	243	29.629	56	138	40.579	28	171	16.374
	82	282	29.078	39	92	42.391	29	143	20.279
	25	121	20.661	39	125	31.2	32	124	25.806
	62	234	26.495	28	132	21.212	36	137	26.277
				30	103	29.126	33	113	29.203

	D4	D6	D10
mean	22.66207143	32.8742	18.32086667
sd	4.190494362	6.450151318	5.791062595
SEM	1.119956727	1.665421909	1.495245933

	D4									D6										D10								
	Positive Cells	Total cells	%			Positive Cells	Total cells	%			Positive Cells	Total cells	%			Positive Cells	Total cells	%			Positive Cells	Total cells	%			Positive Cells	Total cells	%
PAX7	98	306	32.026		OLIG2	3	306	0.98		PAX7	62	105	59.047		OLIG2	0	105	0		PAX7	190	250	76		OLIG2	8	250	3.2
	60	307	19.543			0	307	0			55	120	55			0	120	0			196	300	65.333			15	300	5
	109	295	36.949			2	295	0.677			32	88	32			0	88	0			182	248	73.387			7	248	2.822
	119	304	39.144			6	304	1.973			40	118	33.898			3	118	2.54			80	158	50.632			10	158	6.329
	80	290	27.586			4	290	1.379			45	90	50			0	90	0			92	153	60.13			9	153	5.882
	123	339	36.283			3	339	0.884			41	80	51.25			0	80	0			110	185	59.459			7	185	3.783
	206	551	37.386			10	551	1.814			60	128	46.875			2	128	1.562			120	199	60.301			10	199	5.025
	159	500	31.8			13	500	2.6			55	116	47.413			3	116	2.586			110	180	61.111			12	180	6.666
	85	291	29.209			4	291	1.374			50	90	55.555			0	90	0			126	228	55.263			13	228	5.701
	125	339	36.873			5	339	1.474			39	60	65			0	60	0			80	138	57.971			18	138	13.043
	88	310	28.387			3	310	0.967			45	80	56.25			1	80	1.25			81	125	64.8			14	125	11.2
	105	320	32.812			6	320	1.875			42	65	64.615			1	65	1.538			76	108	70.37			8	108	7.407
	155	402	38.557			30	402	7.462			60	105	57.142			0	105	0			115	142	80.985			9	142	6.338
	115	313	36.741			9	313	2.875			65	90	72.222			0	90	0			60	90	66.666			9	90	10
											42	88	47.727			0	88	0			120	175	68.571			12	175	6.857

	D4		D6		D10	
	PAX7	OLIG2	PAX7	OLIG2	PAX7	OLIG2
mean	33.09257143	1.881	52.93293333	0.631733333	64.73193333	6.616866667
sd	5.488390709	1.775240655	10.81540754	0.982725035	8.161667463	2.868857958
SEM	1.466834117	0.474453022	2.792522622	0.253738513	2.107333478	0.740735939

Table 1. Figure 1 quantification

	D6					D10					D14		
	Positive Cells	Total cells	%			Positive Cells	Total cells	%			Positive Cells	Total cells	%
SOX10	3	109	2.752			38	141	26.95			52	215	24.186
	3	103	2.912			72	223	32.286			34	211	16.113
	0	112	0			60	256	23.437			53	189	28.042
	0	151	0			35	183	19.125			57	249	22.891
	0	96	0			45	202	22.277			48	263	18.25
	3	122	2.459			40	215	18.604			62	213	29.107
	0	120	0			25	185	12.513			85	222	38.288
	0	139	0			15	166	9.036			55	212	25.943
	4	102	3.921			21	156	13.461			48	238	20.168
	0	114	0			75	161	46.583			37	187	19.786
	3	121	2.479			80	181	44.198			41	242	16.942
	1	126	0.793			72	152	47.368			31	182	17.032
	2	115	1.739			35	211	16.587			65	201	32.338
	0	112	0			29	192	15.104			27	197	13.705
	9	111	8.108			48	203	23.645			21	230	9.13

	D6	D10	D14
mean	1.677533333	24.74493333	22.12806667
sd	2.248816732	12.50822433	7.661348785
SEM	0.580641984	3.229609635	1.97815175

n=3 independent differentiations

N=15 neural rosettes (5 rosettes per differentiation)

	D6					D10					D14		
	Positive Cells	Total cells	%			Positive Cells	Total cells	%			Positive Cells	Total cells	%
TFAP2a	3	109	2.752			36	141	25.531			49	215	22.79
	3	103	2.912			58	223	26.008			27	211	12.796
	0	112	0			60	256	23.437			39	189	20.634
	0	151	0			32	183	17.486			56	249	22.489
	0	96	0			35	202	17.326			48	263	18.25
	2	122	1.639			39	215	18.139			46	213	21.596
	0	120	0			25	185	13.513			65	222	29.279
	0	139	0			12	166	7.228			45	212	21.226
	1	102	0.98			21	156	13.461			36	238	15.126
	3	114	2.631			74	161	45.962			36	187	19.251
	4	121	3.305			71	181	39.226			35	242	14.462
	0	124	0			68	152	44.736			28	182	15.384
	0	91	0			32	211	15.165			41	201	20.398
	0	82	0			29	192	15.104			30	197	15.228
	0	108	0			42	203	20.689			31	230	13.478

	D6	D10	D14
mean	0.947933333	22.8674	18.8258
sd	1.311119776	11.72124353	4.47669274
SEM	0.33852967	3.026412065	1.155877095

	D6										D8										D10										D14										D20							
	Positive Cells	Total Cells	%			Positive Cells	Total Cells	%			Positive Cells	Total Cells	%			Positive Cells	Total Cells	%			Positive Cells	Total Cells	%			Positive Cells	Total Cells	%			Positive Cells	Total Cells	%			Positive Cells	Total Cells	%			Positive Cells	Total Cells	%			Positive Cells	Total Cells	%
DCX	0	177	0	NFIA	0	177	0	DCX	7	157	4.458	NFIA	0	157	0	DCX	80	230	34.782	NFIA	0	230	0	DCX	198	364	54.395	NFIA	1	364	0.274	DCX	38	168	22.619	NFIA	45	168	26.785
	3	152	1.973		0	152	0		18	145	12.413		0	145	0		78	241	32.365		0	241	0		92	227	40.528		0	227	0		49	200	24.5		24	200	12
	1	145	0.689		0	145	0		19	110	17.272		1	110	0.909		58	145	40		0	145	0		83	201	41.293		0	201	0		71	222	31.981		22	222	9.909
	0	172	0		0	172	0		18	106	16.981		0	106	0		64	186	34.408		0	186	0		168	325	51.692		0	325	0		67	190	35.263		32	190	16.842
	3	155	1.935		0	155	0		12	139	8.63 3		1	139	0.719		121	330	36.666		5	330	1.515		78	181	43.093		0	181	0		47	135	34.814		10	135	7.407
	1	139	0.719		0	139	0		14	105	13.333		0	105	0		112	297	37.71		2	297	0.673		89	209	42.583		0	209	0		34	101	33.663		20	101	19.801
	0	159	0		0	159	0		15	132	11.363		1	132	0.757		48	166	28.915		2	166	1,2		63	125	50.4		0	125	0		25	94	26.595		16	93	17.204
	1	135	0.74		0	135	0		14	154	9.09		0	154	0		42	162	25.925		3	162	1.851		152	280	54.285		0	280	0		40	138	28.985		14	138	10.144
	1	145	0.689		0	145	0		21	153	13.725		0	153	0		57	180	31.666		0	180	0		85	180	47.222		0	180	0		23	120	19.166		20	120	16.666
	0	162	0		0	162	0		15	146	10.273		0	146	0		48	172	27.906		0	172	0		68	135	50.37		0	135	0		68	194	35.051		12	194	6.185
	1	175	0.571		0	175	0		12	127	9.448		0	127	0		61	165	36.969		0	165	0		95	225	42.222		0	225	0		42	126	33.333		18	126	14.285
	2	190	1.052		0	190	0		12	101	11.881		0	101	0		41	193	21.243		2	193	1.036		98	211	46.445		0	211	0		56	178	31.46		14	178	7.865
	0	162	0		0	162	0		15	137	10.948		1	137	0.729		28	137	20.437		0	137	0		78	178	43.82		0	178	0		71	230	30.869		39	230	16.956
	0	171	0		0	171	0		12	146	8.219		0	146	0		49	172	28.488		0	172	0		125	233	53.648		0	233	0		55	152	36.184		17	152	11.184
	0	155	0		0	155	0		15	141	10.638		0	141	0		69	201	34.328		1	201	0.497		112	215	52.093		0	215	0		56	180	31.11		7	180	3.888

	D6		D8		D10		D14		D20	
	DCX	NFIA	DCX	NFIA	DCX	NFIA	DCX	NFIA	DCX	NFIA
mean	0.557866667	0	11.245	0.2076	31.45386667	0.451466667	47,6059333	0.018266667	30.372933333	13.1414
sd	0.676940266	0	3.304071925	0.358694617	5.872021395	0,647926789	5.069843636	0.074960496	5.069818966	6.025462221
SEM	0.174785225	0	0.853107703	0.092614552	1.516149405	0,167293978	1.309027998	0.018266667	1.309021628	1.555767656

Table 2A. Figure 2 quantification

	D6			D8			D10			D14		
	Positive Cells	Total Cells	%	Positive Cells	Total Cells	%	Positive Cells	Total Cells	%	Positive Cells	Total Cells	%
P27	0	93	0	10	121	8.264	26	116	22.413	60	175	34.285
	0	89	0	10	104	9.615	18	107	16.822	57	162	35.185
	0	109	0	8	94	8.51	28	101	27.722	49	139	35.251
	0	118	0	11	94	11.702	29	115	25.217	39	149	26.174
	0	96	0	9	96	9.375	24	104	23.076	45	145	31.034
	0	88	0	12	108	11.111	33	119	27.731	56	136	41.176
	0	83	0	15	123	12.195	51	120	42.5	43	146	29.452
	0	84	0	11	104	10.576	49	109	44.954	54	150	36
	2	114	1.754	7	114	6.14	26	95	27.368	44	144	30.555
	0	95	0	6	95	6.315	22	78	28.205	64	148	43.243
	2	105	1.904	12	115	10.434	26	114	22.807	65	157	41.401
	0	103	0	10	103	9.708	27	103	26.213	61	167	36.526
	1	92	1.086	13	112	11.607	31	116	29.31	65	136	47.794
	0	86	0	10	96	10.416	26	105	24.761	69	157	43.949
	0	98	0	11	98	11.224	28	118	23.728	81	172	47.093

	D6	D8	D10	D14
mean	0.316266667	9.8128	27.5218	37.27453333
sd	0.675106284	1.842630891	7.288052956	6.5877314 1
SEM	0.174311693	0.47576525	1.881767182	1.700944936

	D6			D10			D14		
	Positive Cells	Total cells	%	Positive Cells	Total cells	%	Positive Cells	Total cells	%
LHX2	1	120	0.833	43	212	20.283	41	177	23.163
	0	132	0	19	160	11.875	38	168	22.619
	0	109	0	21	166	12.65	49	175	28
	0	106	0	9	106	8.49	51	215	23.72
	0	118	0	6	111	5.405	36	205	17.561
	0	96	0	12	101	11.881	55	225	24.444
	0	111	0	15	127	11.811	69	227	30.396
	0	104	0	9	107	8.411	65	216	30.092
	0	95	0	21	136	15.441	60	265	22.641
	0	118	0	15	105	14.285	40	202	19.801
	0	110	0	18	103	17.475	27	210	12.857
	0	95	0	17	115	14.782	40	230	17.391
	0	93	0	9	75	12	35	250	14
	0	85	0	9	90	10	49	275	17.818
	0	101	0	11	85	12.941	48	267	17.977

	D6	D10	D14
mean	0.055533333	12.51533333	21.49866667
sd	0.215079675	3.71742952	5.387370849
SEM	0.055533333	0.959836175	1.391013172

	D6									D10									D14								
	Positive Cells	Total cells	%			Positive Cells	Total cells	%			Positive Cells	Total cells	%			Positive Cells	Total cells	%			Positive Cells	Total cells	%			Positive Cells	Total cells	%
ISLET1	1	90	1.111		HB9	0	90	0		ISLET1	15	144	10.416		HB9	0	144	0		ISLET1	30	246	12.195		HB9	0	246	0
	0	116	0			0	116	0			7	140	5			0	140	0			38	190	20			0	190	0
	2	87	2.298			0	87	0			15	132	11.363			0	132	0			29	150	19.333			0	150	0
	0	100	0			0	100	0			27	240	11.25			0	240	0			35	171	20.467			0	171	0
	0	111	0			0	111	0			15	190	7.894			0	190	0			38	175	21.714			0	175	0
	0	100	0			0	100	0			18	198	9.09			0	198	0			46	148	31.081			0	148	0
	0	94	0			0	94	0			10	190	5.263			0	190	0			49	204	24.019			0	204	0
	0	102	0			0	102	0			16	174	9.195			0	174	0			46	214	21.495			0	214	0
	0	119	0			0	119	0			21	180	11.666			0	180	0			57	172	33.139			0	172	0
	0	101	0			0	101	0			7	134	5.223			0	134	0			39	200	19.5			0	200	0
	0	105	0			0	105	0			22	186	11.827			0	211	0			41	210	19.523			0	210	0
	0	96	0			0	96	0			15	211	7.109			0	186	0			37	170	21.764			0	170	0
	0	117	0			0	117	0			13	157	8.28			0	157	0			31	221	14.027			0	221	0
	0	122	0			0	122	0			11	156	7.051			0	156	0			31	191	16.231			0	191	0
	0	109	0			0	109	0			1	204	0.491			0	204	0			41	205	20			0	205	0

	D6		D10		D14	
	ISLET1	HB9	ISLET1	HB9	ISLET1	HB9
mean	0.227266667	0	8.074533333	0	20.96586667	0
sd	0.640333224	0	3.170170159	0	5.462900235	0
SEM	0.165333328	0	0.818534415	0	1.410514776	0

	D6			D10			D14		
	Positive Cells	Total cells	%	Positive Cells	Total cells	%	Positive Cells	Total cells	%
BRN3A	0	90	0	0	134	0	17	221	7.692
	0	116	0	5	186	2.688	12	191	6.282
	0	87	0	3	211	1.421	26	205	12.682
	0	100	0	0	157	0	32	196	16.326
	0	111	0	0	156	0	28	213	13.145
	0	100	0	2	204	0.98	18	168	10.714
	0	94	0	0	163	0	26	170	15.294
	0	102	0	0	185	0	23	157	14.649
	0	119	0	0	108	0	26	134	19.402
	0	101	0	0	115	0	14	128	10.937
	0	105	0	0	120	0	31	145	21.379
	0	96	0	0	167	0	17	125	13.6
	0	117	0	0	181	0	23	151	15.231
	0	122	0	1	156	0.641	13	120	10.833
	0	109	0	0	161	0	21	128	16.406

	D6	D10	D14
mean	0	0.382	13.63813333
sd	0	0.775840834	4.041510801
SEM	0	0.200321242	1.043513602

Table 2B. Figure 2 quantification

	SOX2+	Total GFP+	%		
incorporated cells	22	22	100		
	28	28	100		
	18	20	90	mean	93.6715
	16	19	84,21	sd	6.217388383
	25	26	96,153		
	22	24	91,666		
individual cells	2	3	66.666		
	2	3	66.666		
	0	5	0	mean	47.49966667
	1	6	16.666	sd	31.1581664
	3	4	75		
	3	5	60		
contiguous rosette	5	5	100		
	3	3	100		
	16	16	100	mean	96.27216667
	13	14	92.857	sd	4.152548346
	156	171	91.228		
	145	155	93.548		
	n=3 different transplanted chicken embryos				
	3 different sections per markers				

	PAX7+	Total GFP+	%		
incorporated cells	38	40	95		
	34	35	97.142		
	10	10	100	mean	92.982
	8	10	80	sd	6.938540481
	23	25	92		
	30	32	93.75		
individual cells	5	7	71.428		
	3	3	100		
	0	1	0	mean	58.5712
	5	7	71.428	sd	37.25248656
	1	2	50		
contiguous rosette	110	120	91.666		
	90	91	98.901		
	37	37	100	mean	96.8634
	30	32	93.75	sd	3.890197913
	1	1	100		

	P27+	Total GFP+	%		
incorporated cells	3	15	20		
	7	40	17.5		
	3	35	8.571	mean	13.0895
	10	80	12.5	sd	5.30865255
	1	17	5.882		
	10	71	14.084		
individual cells	2	4	50		
	2	5	40		
	2	3	66.666	mean	38.33316667
	2	5	40	sd	22.08553574
	1	3	33.333		
	0	4	0		
contiguous rosette	5	20	25		
	10	60	16.666		
	7	120	5.833	mean	15.95983333
	13	46	28.26	sd	11.01915936
	4	20	20		
	0	10	0		

	ISLET1+	Total GFP+	%		
incorporated cells	0	10	0		
	0	19	0		
	0	24	0	mean	0
	0	31	0	sd	0
	0	19	0		
individual cells	0	6	0		
	0	1	0		
	0	1	0	mean	0
	0	1	0	sd	0
	0	6	0		
contiguous rosette	0	45	0		
	0	205	0		
	0	10	0	mean	0
	0	21	0	sd	0
	0	40	0		

Table 3. Figure 4 quantification

	SNAI2+	Total GFP+	%		
incorporated cells	11	61	18.032		
	2	10	20		
	2	19	10.526	mean	12.55116667
	1	8	12.5	sd	5.462052816
	1	13	7.692		
	4	61	6.557		
individual cells	3	5	60		
	1	3	33.333		
	1	2	50	mean	51.6665
	0	2	0	sd	33.58237964
	2	2	100		
	2	3	66.666		
contiguous rosette	8	47	17.021		
	3	37	8.108		
	5	22	22.727	mean	15.5712
	1	10	10	sd	6.317817796
	1	5	20		
		n=3 different transplanted chicken embryos			
		3 different sections per markers			

	HNK1+	Total GFP+	%		
incorporated cells	8	101	7.92		
	4	82	4.878		
	3	58	5.172	mean	6.0592
	2	30	6.666	sd	1.242225905
	3	53	5.66		
individual cells	5	9	55.555		
	1	4	25		
	3	7	42.857	mean	51.349
	2	2	100	sd	29.47698406
	1	3	33.333		
contiguous rosette	7	30	23.333		
	6	34	17.647	mean	19.099
	3	16	18.75	sd	2.948239588
	3	18	16.666		

	TFAP2a+	Total GFP+	%		
incorporated cells	2	13	15.384		
	11	64	17.187		
	6	50	12	mean	11.50033333
	10	82	12.195	sd	5.06104233
	3	107	2.803		
	5	53	9.433		
individual cells	4	6	66.666		
	4	10	40		
	0	4	0	mean	41.94433333
	3	4	75	sd	28.33158295
	2	4	50		
	1	5	20		
contiguous rosette	8	109	7.339		
	10	113	8.849		
	4	49	8.163	mean	13.5995
	10	49	20.408	sd	6.397391398
	8	37	21.621		
	7	46	15.217		

Table 4. Figure 5 quantification

	SOX2+ cells	Total GFP+	%		
Incorporated cells	107	107	100		
	28	28	100		
	139	139	100		
	97	103	94.174	mean	95.86522222
	90	103	87.378	sd	5.018030435
	87	87	100		
	98	111	88.288		
	56	58	96.551		
	107	111	96.396		
individual cells	4	5	80		
	0	0	0		
	26	30	86.666		
	20	26	76.923	mean	54.80022222
	28	34	82.352	sd	38.38133378
	0	0	0		
	1	8	12.5		
	5	7	71.428		
	30	36	83.333		
		n=3 different transplanted chicken embryos			
		3 different sections per markers			

	PAX7+ cells	Total GFP+	%		
Incorporated cells	88	96	91.666		
	184	194	94.845		
	92	98	93.877		
	10	10	100	mean	77.25233333
	170	238	71.428	sd	26.90855654
	119	234	50.854		
	12	66	18.181		
	181	195	92.82		
	102	125	81.6		
Individual cells	8	8	100		
	6	6	100		
	0	0	0		
	0	6	0	mean	63.8446
	36	47	76.595	sd	40.93906927
	4	20	20		
	3	3	100		
	23	27	85.185		
	5	6	83.333		
	11	15	73.333		

	P27+ cells	Total GFP+	%		
Incorporated cells	13	174	7.471		
	14	240	5.833		
	3	55	5.454		
	16	175	9.142	mean	6.646444444
	17	184	9.239	sd	1.59168253
	2	40	5		
	9	146	6.164		
	8	136	5.882		
	4	71	5.633		
individual cells	0	6	0		
	0	9	0		
	1	18	5.555		
	1	16	6.25	mean	3.331555556
	1	16	6.25	sd	3.186384868
	0	3	0		
	1	19	5.263		
	1	15	6.666		
	0	4	0		

	ISLET1+ cells	Total GFP+	%		
Incorporated cells	2	23	8.695		
	10	287	3.484		
	3	129	2.325		
	5	71	7.042	mean	5.002444444
	10	171	5.847	sd	2.176657076
	4	65	6.153		
	5	210	2.381		
	6	112	5.357		
	4	107	3.738		
Individual cells	0	2	0		
	0	0	0		
	0	0	0		
	0	6	0	mean	0
	0	6	0	sd	0
	0	7	0		
	0	1	0		
	0	10	0		
	0	6	0		

Table 5A. Figure 6 quantification

ChiPS4-pmGFP		2DPO-D08				5DPO-D11	
		SOX2				SOX2	
	SOX2+	Total	%		SOX2+	Total	%
	90	99	90.9		147	174	84.482
	88	102	86.27		115	150	76.666
	98	115	85.217		147	169	86.982
	118	130	90.769		213	233	91.416
	58	95	61.052		105	155	67.741
	87	99	87.878		140	171	81.871
	83	101	82.178		141	151	93.377
	101	119	84.873		89	111	80.18
	120	129	93.023		198	215	92.093
	115	122	94.262		131	164	79.878
	80	95	84.21		171	208	82.211
	99	110	90		172	205	83.902
	82	103	79.611		190	230	82.608
	78	101	77.227		165	204	80.882
	115	132	87.121		196	212	92.452
	mean	84.97273333			mean	83.78273333	
	sd	8.147069425			sd	6.852543787	
	SEM	2.10356428			SEM	1.769319198	
		n=3 independent differentiations					
		N=15 neural rosettes (5 rosettes per differentiation)					

ChiPS4-pmGFP		2DPO-D08				5DPO-D11	
		PAX7				PAX7	
	PAX7+	Total	%		PAX7+	Total	%
	60	103	58.252		122	151	80.794
	55	120	45.833		200	270	74.074
	42	98	42.857		157	201	78.109
	65	128	50.781		120	168	71.428
	66	100	66		104	160	65
	52	90	57.777		170	220	77.272
	71	138	51.449		134	180	74.444
	67	116	57.758		126	181	69.613
	60	100	60		125	171	73.099
	69	90	76.666		146	200	73
	65	100	65		174	250	69.6
	72	95	75.789		203	300	67.666
	70	115	60.869		181	248	72.983
	76	100	76		101	158	63.924
	73	118	61.864		126	228	55.263
	mean	60.45966667			mean	71.0846	
	sd	10.38827646			sd	6.370944646	
	SEM	2.682241448			SEM	1.644970834	

ChiPS4-pmGFP		2DPO-D08				5DPO-D11	
		P27				P27	
	P27+	Total	%		P27+	Total	%
	10	121	8.264		30	145	20.689
	10	104	9.615		25	146	17.123
	8	94	8.51		30	245	12.244
	11	94	11.702		23	170	13.529
	9	96	9.375		22	125	17.6
	12	108	11.111		29	170	17.058
	15	123	12.195		26	150	17.333
	11	104	10.576		28	149	18.791
	7	114	6.14		24	140	17.142
	6	95	6.315		24	153	15.686
	12	115	10.434		35	145	24.137
	10	103	9.708		29	138	21.014
	13	112	11.607		33	121	27.272
	10	96	10.416		51	145	35.172
	11	98	11.224		31	126	24.603
	mean	9.8128			mean	19.95953333	
	sd	1.842630891			sd	5.873229215	
	SEM	0.47576525			SEM	1.516461262	

ChiPS4-pmGFP		2DPO-D08				5DPO-D11	
		ISLET1				ISLET1	
	ISLET1+	Total	%		ISLET1+	Total	%
	0	162	0		5	65	7.692
	0	175	0		7	80	8.75
	0	166	0		5	68	7.352
	0	59	0		15	100	15
	0	60	0		9	81	11.111
	0	59	0		3	55	5.455
	0	89	0		7	55	12.727
	0	98	0		4	50	8
	0	88	0		10	100	10
	0	125	0		23	153	15.032
	0	120	0		25	155	16.129
	0	119	0		13	156	8.333
	0	132	0		15	132	11.363
	0	140	0		7	134	5.223
	0	127	0		7	140	5
	mean	0			mean	9.811133333	
	sd	0			sd	3.655095619	
	SEM	0			SEM	0.943741631	

Table 5B. Figure 6 quantification

	SNAI2+ cells	Total GFP+	%		
Incorporated cells	0	150	0		
	0	185	0		
	0	16	0		
	0	144	0	mean	0
	0	49	0	sd	0
	0	22	0		
	0	12	0		
	0	126	0		
	0	29	0		
	0	81	0		
	0	46	0		
Individual cells	0	3	0		
	0	7	0		
	0	6	0		
	0	12	0	mean	0
	0	3	0	sd	0
	0	9	0		
	0	6	0		
	0	14	0		
	0	3	0		
	0	7	0		
	0	0	0		
	n=3 different transplanted chicken embryos				
	3 different sections per markers				

	HNK1+ cells	Total GFP+	%		
Incorporated cells	0	157	0		
	0	190	0		
	0	56	0		
	0	134	0	mean	0
	0	69	0	sd	0
	0	36	0		
	0	25	0		
	0	116	0		
	0	59	0		
	0	51	0		
	0	63	0		
Individual cells	0	3	0		
	0	6	0		
	0	5	0		
	0	8	0	mean	0
	0	4	0	sd	0
	0	7	0		
	0	9	0		
	0	10	0		
	0	1	0		
	0	4	0		
	0	0	0		

	TFAP2a+ cells	Total GFP+	%		
Incorporated cells	0	165	0		
	0	180	0		
	0	85	0		
	0	154	0	mean	0
	0	80	0	sd	0
	0	51	0		
	0	75	0		
	0	135	0		
	0	80	0		
	0	75	0		
	0	95	0		
Individual cells	0	15	0		
	0	4	0		
	0	6	0		
	0	4	0	mean	0
	0	3	0	sd	0
	0	4	0		
	0	3	0		
	0	5	0		
	0	6	0		
	0	12	0		
	0	4	0		

Table 6. Figure 7 quantification

ChiPS4-pmGFP																					
D06-D0		SOX2			PAX7				SNAI2				P27				ISLET1				TFAP2a	
	SOX2+	Total	%	PAX7+	Total	%		SNAI2+	Total	%		P27+	Total	%		ISLET1+	Total	%		TFAP2a+	Total	%
	167	212	78.777	103	164	62.805		40	120	33.333		0	204	0		0	97	0		0	105	0
	176	226	77.876	99	155	63.87		28	80	35		0	201	0		0	120	0		0	115	0
	175	221	79.185	101	162	62.345		37	125	29.6		0	200	0		0	134	0		0	97	0
	187	219	85.388	186	286	65.034		50	155	32.258		0	125	0		0	151	0		0	120	0
	174	206	84.466	191	282	67.73		37	120	30.833		0	120	0		0	120	0		0	85	0
	176	209	84.21	176	276	63.768		65	151	43.046		0	119	0		0	101	0		0	105	0
	261	301	86.711	48	87	55.172		55	181	30.386		0	38	0		0	165	0		0	103	0
	220	284	77.464	53	86	61.627		25	104	24.038		0	40	0		0	145	0		0	135	0
	238	287	82.926	40	79	50.632		31	129	24.031		0	38	0		0	110	0		0	107	0
	141	161	87.577	88	140	62.857		53	184	28.804		0	99	0		0	94	0		0	145	0
	143	178	80.337	63	131	48.091		75	284	26.408		0	91	0		0	100	0		0	120	0
	147	171	85.965	81	130	62.307		20	100	20		0	73	0		0	103	0		0	110	0
	88	96	91.666	69	124	55.645		17	65	26.153		0	132	0		0	95	0		0	90	0
	81	100	81	74	128	57.812		28	168	16.666		0	140	0		0	102	0		0	101	0
	84	113	74.336	123	219	56.164		25	121	20.661		0	127	0		0	85	0		0	111	0
	mean		82.5256	mean		59.72393333		mean		28.08113333		mean		0		mean		0		mean		0
	sd		4.629129566	sd		5.567674681		sd		6.668137916		sd		0		sd		0		sd		0
	SEM		1.195236115	SEM		1.437567421		Sem		1.721705807		SEM		0		SEM		0		SEM		0
				n=3 independent differentiations																		
				N=15 neural rosettes (5 per differentiation)																		

ChiPS4-pmGFP																					
D08-2DPO		SOX2			PAX7				SNAI2				P27				ISLET1				TFAP2a	
	SOX2+	Total	%	PAX7+	Total	%		SNAI2+	Total	%		P27+	Total	%		ISLET1+	Total	%		TFAP2a+	Total	%
	90	99	90.9	60	103	58.252		20	102	19.607		10	121	8.264		0	162	0		14	90	15.555
	88	102	86.27	55	120	45.833		24	97	24.742		10	104	9.615		0	175	0		16	108	14.814
	98	115	85.217	42	98	42.857		19	101	18.811		8	94	8.51		0	166	0		17	68	25
	118	130	90.769	65	128	50.781		23	99	23.232		11	94	11.702		0	59	0		16	88	18.181
	58	95	61.052	66	100	66		19	60	31.666		9	96	9.375		0	60	0		10	91	10.989
	87	99	87.878	52	90	57.777		20	81	24.691		12	108	11.111		0	59	0		16	90	17.777
	83	101	82.178	71	138	51.449		20	96	20.833		15	123	12.195		0	89	0		13	96	13.541
	101	119	84.873	67	116	57.758		10	74	13.513		11	104	10.576		0	98	0		8	51	15.686
	120	129	93.023	60	100	60		21	75	28		7	114	6.14		0	88	0		12	77	15.584
	115	122	94.262	69	90	76.666		25	106	23.584		6	95	6.315		0	125	0		10	76	13.157
	80	95	84.21	65	100	65		75	301	33.222		12	115	10.434		0	120	0		26	100	26
	99	110	90	72	95	75.789		78	287	27.177		10	103	9.708		0	119	0		25	106	23.584
	82	103	79.611	70	115	60.869		27	100	27		13	112	11.607		0	132	0		18	107	16.822
	78	101	77.227	76	100	76		22	70	31.428		10	96	10.416		0	140	0		12	88	13.636
	115	132	87.121	73	118	61.864		63	184	34.239		11	98	11.224		0	127	0		24	108	22.222
	mean		84.97273333	mean		60.45966667		mean		25.44966667		mean		9.8128		mean		0		mean		17.5032
	sd		8.147069425	sd		10.38827646		sd		5.827383788		sd		1.842630891		sd		0		sd		4.618523113
	SEM		2.10356428	SEM		2.682241448		SEM		1.504624024		SEM		0.47576525		SEM		0		SEM		1.19249754

ChiPS4-pmGFP																					
D11-5DPO		SOX2			PAX7				SNAI2				P27				ISLET1				TFAP2a	
	SOX2+	Total	%	PAX7+	Total	%		SNAI2+	Total	%		P27+	Total	%		ISLET1+	Total	%		TFAP2+	Total	%
	147	174	84.482	122	151	80.794		31	146	21.232		30	145	20.689		5	65	7.692		15	88	17.045
	115	150	76.666	200	270	74.074		20	125	16		25	146	17.123		7	80	8.75		21	114	18.421
	147	169	86.982	157	201	78.109		20	120	16.666		30	245	12.244		5	68	7.352		13	101	12.871
	213	233	91.416	120	168	71.428		15	87	17.241		23	170	13.529		15	100	15		20	118	16.949
	105	155	67.741	104	160	65		11	101	10.891		22	125	17.6		9	81	11.111		18	80	22.5
	140	171	81.871	170	220	77.272		31	146	21.232		29	170	17.058		3	55	5.455		18	100	18
	141	151	93.377	134	180	74.444		30	145	20.689		26	150	17.333		7	55	12.727		14	90	15.555
	89	111	80.18	126	181	69.613		24	135	17.777		28	149	18.791		4	50	8		18	85	21.176
	198	215	92.093	125	171	73.099		19	101	18.811		24	140	17.142		10	100	10		10	86	11.627
	131	164	79.878	146	200	73		21	100	21		24	153	15.686		23	153	15.032		17	107	15.887
	171	208	82.211	174	250	69.6		18	120	15		35	145	24.137		25	155	16.129		20	100	20
	172	205	83.902	203	300	67.666		16	163	9.815		29	138	21.014		13	156	8.333		15	90	16.666
	190	230	82.608	181	248	72.983		25	135	18.518		33	121	27.272		15	132	11.363		16	101	15.841
	165	204	80.882	101	158	63.924		26	146	17.808		51	145	35.172		7	134	5.223		17	110	15.454
	196	212	92.452	126	228	55.263		25	138	18.115		31	126	24.603		7	140	5		19	90	21.111
	mean		83.78273333	mean		71.0846		mean		17.38633333		mean		19.95953333		mean		9.811133333		mean		17.27353333
	sd		6.852543787	sd		6.370944646		sd		3.437058266		sd		5.873229215		sd		3.655095619		sd		3.030563052
	SEM		1.76931998	SEM		1.644970834		SEM		0.887444628		SEM		1.516461262		SEM		0.943741631		SEM		0.782488015

Table 7. Figure S2 quantification

Quality control and passage numbers for pluripotent cells used in this study

H9 (WA09) hES cells were purchased from Wicell and were supplied at passage 24. The cells were thawed and cell banks prepared at passage 29. For experiments the cells were used between passage 29 and 39.

H1 (WA01) hES cells were purchased from Wicell and were supplied at passage 30. The cells were thawed and cell banks prepared at passage 34. For experiments the cells were used between passage 34 and 44.

H1-*DOUBLECORTIN-CITRINE* cells were obtained from the Allen Institute and were supplied at passage 63. The cells were thawed and cell banks prepared at passage 66. For experiments the cells were used between passage 66 and 76.

ChiPS4 hiPS cells were purchased from Cellartis AB and were supplied at passage 9. The cells were thawed and cell banks prepared at passage 13. For experiments the cells used between passage 13 and 23.

To make ChiPS4-pmGFP, the cells were transfected with the PiggyBac and transposase constructs at passage 17 and GFP +ve cells selected by fluorescence activated cell sorting at passage 19. The polyclonal cell line was banked at passage 23. For experiments the cells were used between passage 23 and 33.

For quality control purposes, representative lots of each cell bank were thawed and tested for post-thaw viability, and to ensure sterility and absence of mycoplasma contamination. After 2 passages the cell lines were tested to check for the uniform expression of pluripotency markers (Oct4, Sox2, Nanog, SSEA-3, SSEA-4, TRA-1-60 and TRA-1-81) and absence of differentiation markers (SSEA-1, HNF-3 beta, beta-III-tubulin and smooth muscle alpha-actinin) by immunofluorescence.